

Single Domain Antibody Fragments as New Tools for the Detection of Neuronal Tau Protein in Cells and in Mice Studies

Elian Dupré, Clément Danis, Alexis Arrial, Xavier Hanoulle, Mégane Homa, François-Xavier Cantrelle, Hamida Merzougui, Morvane Colin, Jean-Christophe Rain, Luc Buée, et al.

▶ **To cite this version:**

Elian Dupré, Clément Danis, Alexis Arrial, Xavier Hanoulle, Mégane Homa, et al.. Single Domain Antibody Fragments as New Tools for the Detection of Neuronal Tau Protein in Cells and in Mice Studies. ACS Chemical Neuroscience, 2019, 10 (9), pp.3997-4006. 10.1021/acschemneuro.9b00217 . hal-02337161

HAL Id: hal-02337161
https://hal.science/hal-02337161

Submitted on 18 Nov 2020

HAL is a multi-disciplinary open access archive for the deposit and dissemination of scientific research documents, whether they are published or not. The documents may come from teaching and research institutions in France or abroad, or from public or private research centers.

L'archive ouverte pluridisciplinaire **HAL**, est destinée au dépôt et à la diffusion de documents scientifiques de niveau recherche, publiés ou non, émanant des établissements d'enseignement et de recherche français ou étrangers, des laboratoires publics ou privés.

Single domain antibody fragments as new tools for detection of the neuronal tau protein in cells and in mice studies

Elian Dupré[1*], Clément Danis[1,2*], Alexis Arrial[3], Xavier Hanoulle[1], Mégane Homa[2], François-Xavier Cantrelle[1], Hamida Merzougui[1], Morvane Colin[2], Jean-Christophe Rain[3], Luc Buée[2§ÿ], Isabelle Landrieu[1§ÿ]

[1]Univ. Lille, CNRS, UMR 8576 - UGSF - Unité de Glycobiologie Structurale et Fonctionnelle, F-59000 Lille, France

[2]Univ. Lille, Inserm, CHU Lille, UMR-S 1172 - JPArc - Centre de Recherche Jean-Pierre AUBERT Neurosciences et Cancer, F-59000 Lille, France

[3]Hybrigenic Services, Paris, France

*, § Equal contributions

ÿCorresponding authors: Dr Luc Buée luc.buee@inserm.fr, Dr Isabelle Landrieu, isabelle.landrieu@univ-lille.fr,

ORCID id:

Elian Dupré : 0000-0001-5281-0337

Clément Danis: 0000-0002-5895-4742,

Xavier Hanoulle: 0000-0002-3755-2680

Morvane Colin 0000-0003-0611-4167

Luc Buée 0000-0002-6261-4230

Isabelle Landrieu 0000-0002-4883-2637

Key words: Variable domain of the heavy-chain only antibodies, nanobodies, tauopathies, Alzheimerôs disease, nuclear magnetic resonance spectroscopy

ABSTRACT

Tau is a neuronal protein linked to pathologies called tauopathies, including Alzheimerôs disease. In Alzheimerôs disease, tau aggregates into filaments leading to the observation of intraneuronal fibrillary tangles. Molecular mechanisms resulting in tau aggregation and in tau pathology spreading through the brain regions are still not fully understood. New tools are thus needed to decipher tau pathways involved in the diseases. In this context, a family of novel single domain antibody fragments, or VHHs, directed against tau were generated and characterized. Among the selected VHHs obtained from screening of a synthetic library, a family of six VHHs shared the same CDR3 recognition loop and recognized the same epitope, located in the C-terminal domain of tau. Affinity parameters characterizing the tau/VHHs interaction were next evaluated using surface plasmon resonance spectroscopy. The equilibrium constants K_D were in the micromolar range but despite conservation of the CDR3 loop sequence, a range of affinities was observed for this VHH family. One of these VHHs, named F8-2, was additionally shown to bind tau upon expression in a neuronal cell line model. Optimization of VHH F8-2 by yeast two-hybrid allowed the generation of an optimized VHH family characterized by lower K_D than the F8-2 wild-type counterpart, and recognizing the same epitope. The optimized VHHs can also be used as antibodies for detecting tau in transgenic mice brain tissues. These results validate the use of these VHHs for *in vitro* studies, but also their potential for in-cell expression, and assays in mouse models, to explore the mechanisms underlying tau physiopathology.

INTRODUCTION

The neuronal tau protein has been historically described as a cytosolic protein principally localized in axons and involved in the regulation of tubulin polymerization and microtubule stability [1]. This early view has been amended by many studies that revealed the multifunctional character of this protein[2]. Tau is involved in several biological processes and show various sub-localization including nuclear compartment, dendrites and extracellular medium[2]. Tau gene comprises 16 exons that, depending on alternative splicing, translate into six isoforms in the human brain[3]. The 441-amino acid residue longest isoform (tau) is divided into 4 domains: N-terminal domain, proline-rich domain (PRD), microtubule-binding domain (MTBD) constituted of 4 partially repeated sequences designated R1 to R4, and finally C-terminal domain.

Tau is well known to be associated with Alzheimerôs disease (AD) and several other neurodegenerative diseases, collectively named tauopathies. In AD, tau is found aggregated into paired helical filaments (PHFs)[4,5], which form the intracellular fibrillary deposits leading to the neurofibrillary tangles (NFTs). Recent cryo-electron microscopy structures have shown that tau filament cores are structurally distinct between tauopathies but are nevertheless mainly composed of the MTBD and a part of the C-terminus[6,7]. Moreover, unidentified tau species could propagate tau pathology by an inter-cellular transfer between neurons, suggesting a prion-like character[8].

These findings generated new hypothesis in the molecular understanding of tauopathies and offer new targets to mitigate the diseases[9]. However, the search for in-depth comprehension and for effective therapies is still a challenging task. Advances in the field require development of new experimental tools that may help to decipher key aspects of tauopathies. Antibodies are powerful tools to investigate tau physiopathology and they additionally represent new therapeutic avenues. Several clinical trials are now focused on tau immunization approaches[10,11], based on the encouraging results of active and passive immunotherapies in mice models of tauopathies. These pre-clinical studies showed reduction in tau pathology, cognitive benefit[12ï15] and even concomitant decrease of the tau and amyloid pathologies[14]

Despite their clear interest, the immunoglobulin G IgG-type antibodies are costly to produce and difficult to use in neurodegenerative diseases affecting the brain, which required crossing the blood

brain barrier. One emerging strategy is the use of fragments of these antibodies, such as single-chain variable fragment (ScFv) or fragment antigen binding (Fab) that conserve the binding properties of IgG-like antibodies but are cheaper to produce, easier to target to the brain and amenable to a large number of modifications and optimizations, depending on their desired uses[16,17].

In line with this strategy, VHHs (Variable domain of the heavy-chain only antibody) or nanobodies, are antibody fragments of small size (13kDa) easily produced in prokaryote recombinant systems. Naturally occurring antibodies only composed of the equivalent of the IgG heavy chain are found in *Camelidae*[18]. VHHs correspond to the variable antigen-binding domain of these single chain antibodies[19]. The VHH single domain includes 4 conserved parts called frameworks (FRs) and 3 variable loops called complementary determined regions (CDRs) (**Fig. 1**). FRs form the lattice of the VHHs, bearing the CDRs 1-3 that are responsible for the specific binding of the recognized epitope. VHHs have been described to cross the blood-brain-barrier more easily than classic antibodies and they can be modified to penetrate into the cytoplasm of cells and still bind specifically to their target protein[20,21].

Recently, VHHs showed their potential as diagnostic tools to target Aϐ plaques and tau, with an affinity and a specificity very close to antibodies already used for detecting these pathologic features[22]. Given the interest in tau as an immune target, we here generated, characterized and optimized VHHs targeted against tau. A family of VHHs recognizing an epitope in the C-terminal domain was obtained by screening a naive synthetic library, characterized and finally optimized. These VHHs can be used to detect tau in brain tissues, but are additionally reactive in the cell environment. These VHHs will help to decipher tau pathways and are promising to rationalize future assays in immunotherapy.

RESULTS AND DISCUSSION

Identification of a family of VHHs binding to an epitope in the C-terminal domain of tau

A synthetic phage-display library of humanized llama single-domain antibody[23] was screened against a preparation of biotinylated recombinant full-length tau protein, corresponding to its longest isoform (tau 2N4R, hereafter designated as tau). After cross-validation by non-absorbed phage enzyme-linked immunosorbent assay (ELISA), six VHHs sharing the same CDR3 loop were selected for further analysis (**Fig. 1**).

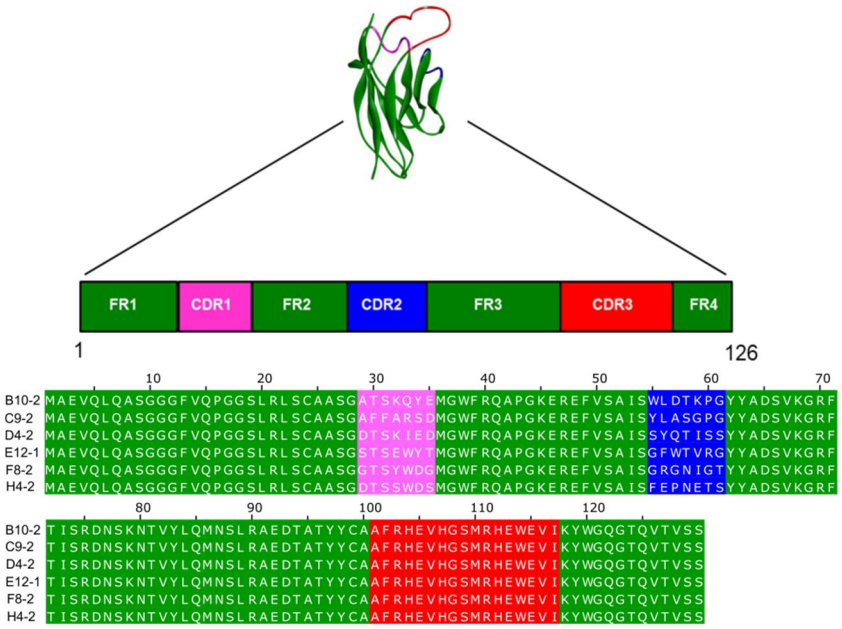


Figure 1 : A family of VHHs share the same CDR3 loop. Structure of a VHH model and alignment of VHH B10-2, C9-2, D4-2, E12-1, F8-2 and H4-2 sequences, showing conservation of the CDR3 loop sequence (in red), but not of the CDR1 and CDR2 loops (in pink and blue, respectively).

We used nuclear magnetic resonance spectroscopy (NMR) to identify the epitope recognized by each VHH, based on resonance perturbation mapping in ^{1}H, ^{15}N heteronuclear single quantum correlation (HSQC) spectra of ^{15}N-tau. Interaction is evidence by a perturbation of resonances, which can be a modification either of the chemical shift value or of the peak intensity, compared to the reference spectrum corresponding to tau in solution. As most of the resonances from the ^{1}H, ^{15}N spectrum of tau have been assigned[24,25] each perturbation can be linked to a specific amino acid residue in tau sequence. The spectrum of ^{15}N-tau in the presence of VHH F8-2 showed a number of resonances broadened beyond detection compared to tau reference spectrum (**Fig. 2a-b**). Intensity ratios of corresponding resonances in these two spectra, plotted along the tau sequence, allowed the identification of the tau C-terminal domain as the target of VHH F8-2 interaction (**Fig. 2c**). A decrease

in the intensity ratio, although to a smaller extent, was additionally observed in tau repeat domains (**Fig. 2c**). Region 370-400 identified as VHH-F8-2 binding site is called Rô repeat, due to its partial sequence homology with repeat R1-R4 sequences, which might explain the presence of a secondary binding site of weak affinity in the MTBD.

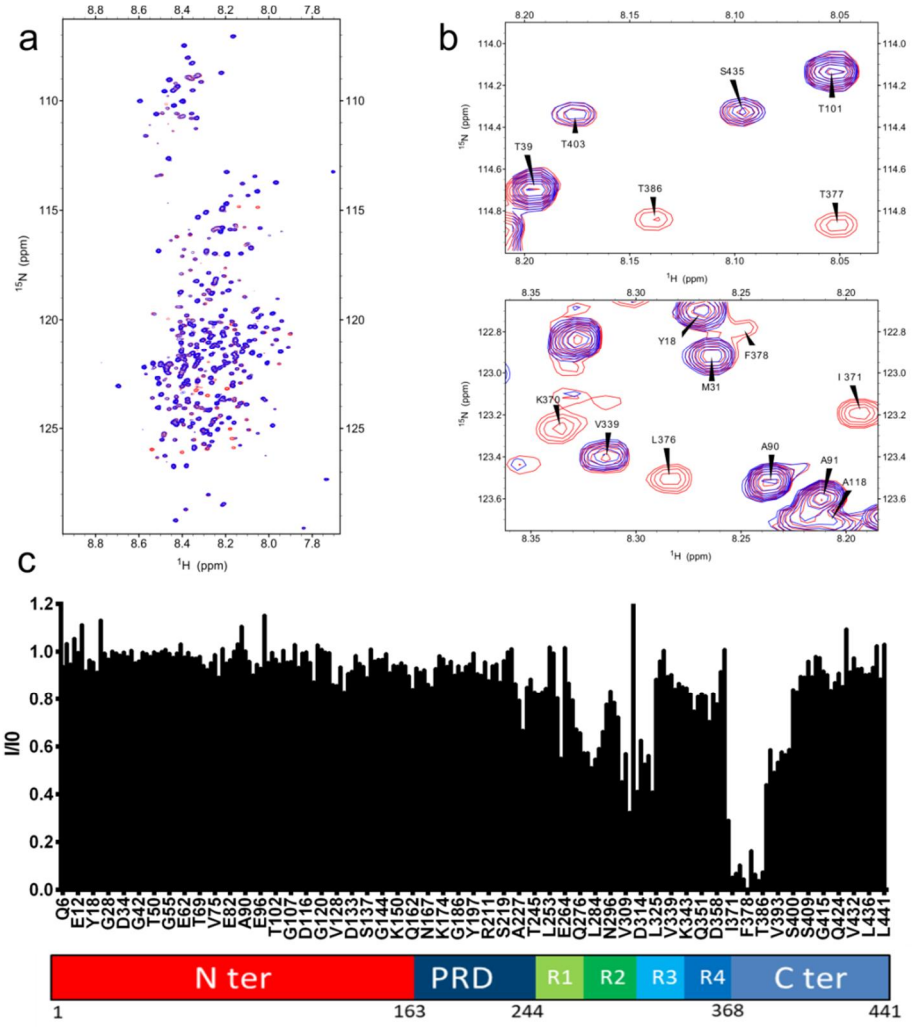


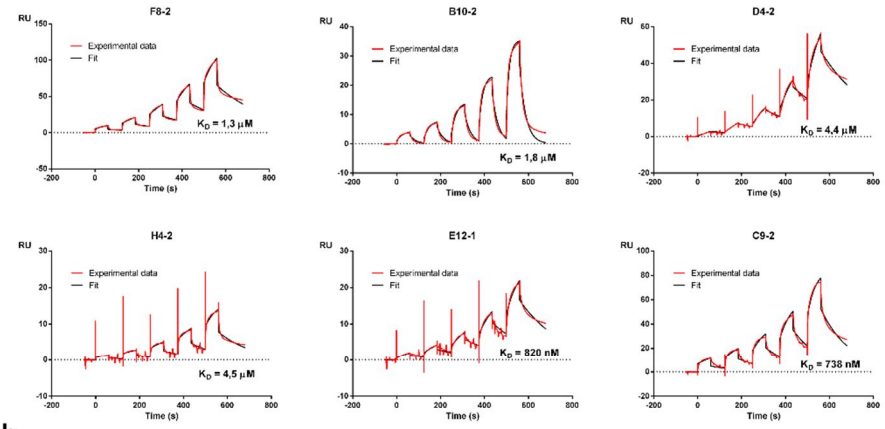
Figure 2: Identification of F8-2 epitope using 2D HSQC NMR experiment. **a.** Superimposition of two-dimensional ^{1}H, ^{15}N HSQC spectra of ^{15}N-tau (in red) with ^{15}N-tau mixed with non-labelled VHH F8-2 (overlaid in blue). **b.** Spectra enlargements show broadened resonances corresponding to residues implicated in the interaction **c.** Normalized intensities I/I0 of corresponding resonances in the two-dimensional spectra of tau with equimolar quantity of VHH F8-2 (I) or free in solution (I0) for residues along the tau sequence. Overlapping resonances are not considered (x-axis is not scaled). Scheme of the 441-amino acid residue longest isoform (tau 2N4R) : N-terminal domain, Nter in red, proline-rich domain, PRD in dark blue, microtubule-binding domain, MTBD constituted of 4 partially repeated sequences designated R1 to R4, and finally C-terminal domain, Cter in light blue. Tau isoforms differ by the presence, or not, of one/two insert(s) in the N-terminal domain (tau 0N, tau 1N and tau 2N), and 3 or 4 repeat sequences in the MTBR (R2 presence or not, tau 3R and tau 4R).

Alternatively, the weak decrease in the intensity ratio in region 264-325 might be due to perturbation of tau conformational ensemble by VHH F8-2 binding in the C-terminal domain. Tau is indeed proposed to adopt a paper-clip conformation involving transient contacts between the C-terminal domain and the repeat region[26]. The five additional VHHs sharing the same CDR3 loop have, as expected, the same epitope that is included in the amino acid sequence $_{370}$KIETHKLTFRENAKAKT$_{386}$ of tau (**Fig.S1-S5**).

The family of VHHs sharing the same CDR3 loop binds to tau with distinct K_D

Another important parameter for recognition by a VHH, besides its epitope, is the affinity that characterizes the binding. Surface plasmon resonance (SPR) experiments were thus next performed to determine the equilibrium dissociation constant associated to VHHs binding to tau. Biotinylated-tau was immobilized on a streptavidin-functionalized sensorchip, allowing the use of a single chip to screen the six different VHHs. The kinetic association (k_{on}) and dissociation (k_{off}) constants and the equilibrium dissociation constant (K_D) were next determined for these tau-VHH complexes (**Fig. 3a**). For the various measured VHH-tau interactions, the K_D ranged from 0.7 ε M to 4.5 ε M (**Fig. 3b**). The K_D here reported to characterize the interaction of the VHHs with tau correspond to one-to-one binding. They can thus not be directly compared to the usual apparent affinity used to define interaction of the IgG, or bivalent fragments derived from the IgG, because in this case the avidity of the antibody is measured, resulting in an apparent higher affinity. Data showed diversity in affinity despite the fact that these VHHs share the same CDR3 loop. These data suggest the importance of the CDR1 and CDR2 loops in the kinetic parameters of the interaction.

a



b

VHH	k_{on} (1/M.s)	k_{off} (1/s)	K_D (nM)	SE (nM)
D4-2	956	0,0042	4421	84,1
C9-2	9839	0,0072	738	12,9
B10-2	19400	0,0358	1846	42,5
E12-1	6635	0,0054	819	18,2
H4-2	1455	0,0066	4502	849
F8-2	3170	0,0042	1332	31,3

Figure 3: Affinity determination for the series of VHHs binding tau by surface plasmon resonance (SPR) **a.** Sensorgrams obtained by single cycle kinetics method of VHHs titrated on immobilized tau. **b.** table of kinetic and thermodynamic constants. Dissociation equilibrium constant K_D is calculated as the ratio of the off-rate on the on-rate k_{off}/k_{on}. Each single cycle kinetics analysis was performed on immobilized biotinylated tau 2N4R (500 resonance units (RU)), with five injections of VHH analyte at 0.25 µM, 0.5 µM, 1 µM, 2 µM and 4 µM.

VHH F8-2 acts as an intrabody in a mouse neuroblastoma cell line

Some VHHs conserve their binding capability once expressed intracellularly, depending on their properties. Indeed, VHHs expressed in cells need both to be able to fold properly and to be stable in the cellular context to retain binding activity[21]. We thus investigated whether VHH F8-2, arbitrarily chosen as the representative of our VHH family, retains its binding potential in the intracellular context. A plasmid coding VHH F8-2 fused to m-Cherry protein (VHH F8-2-m-Cherry), with and without a plasmid coding a plasma membrane-GFP fused to tau protein (GFP-tau), was transfected in mouse neuroblastoma (N2A) cells. Confocal microscopy analysis (40x) showed that cells expressing only VHH F8-2-m-Cherry presented mainly a nuclear labeling (**Fig. 4a**). Plasma membrane-GFP-tau contained a signal peptide addressing the fusion protein to the plasma membranes, avoiding the diffuse localization expected for a standard GFP-tau protein (**Fig. 4b**). This membrane targeting was used in order to facilitate the reading of an interaction of tau with the VHH F8-2-mCherry. For cells expressing both plasma membrane-GFP-tau and VHH F8-2-m-Cherry, the m-Cherry fluorescence was

distributed differently, with almost no labelling of the nucleus (**Fig. 4b**), in a similar manner as the distribution of the green fluorescence of the plasma membrane-GFP-tau (**Fig. 4B**, merged). The VHH F8-2-m-Cherry differential distribution was consistent with recruitment of VHH-F8-2 by tau, due to their interaction (**Fig. 4b**). We concluded that VHH F8-2 retains its binding capability to tau once expressed in the neuroblastoma cells.

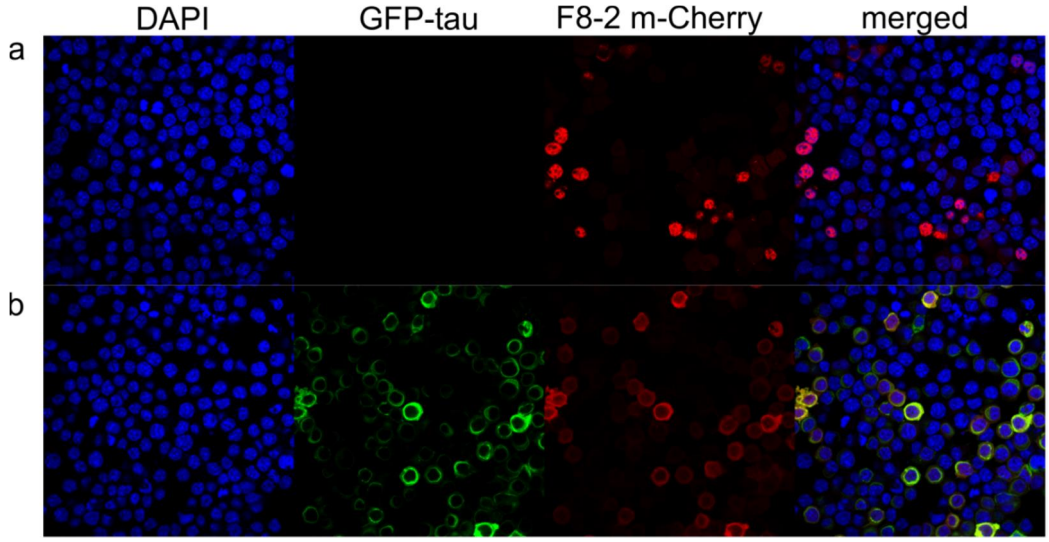


Figure 4: VHH F8-2 acts as an intrabody. Confocal analysis of N2A neuroblastoma cells transfected with plasmids expressing **a.** VHH-F8-2-mCherry or **b.** both VHH F8-2-mCherry and plasma membrane-GFP-tau. DAPI staining was used to visualized cell nuclei.

VHH F8-2 binds to tau peptide $_{373}$THKLTF$_{378}$

NMR and crystallographic studies of VHH-peptide complexes have indicated that a limited number of residues constitute the bound epitope, which does not exceed 5 to 8 amino acids[27,28]. In particular, the disordered epitopes were proposed to be short, in order to have a limited interface with antibodies while retaining affinity and specificity, to compensate for the entropic cost of order gain due to the binding[29]. The binding site identified by NMR for VHH F8-2 was thus larger than expected for an epitope, about 17 contiguous amino-acid residues showing strong reduction of their resonance intensities (residues 370 to 386, **Fig. 2c**). However, NMR epitope mapping by resonance intensity decrease does not allow identification of the residues in a direct interaction, but rather the region of the protein affected by the binding. The decrease in resonance intensity can indeed result from local immobilization of the disordered protein due to the binding, decreasing local tumbling and increasing relaxation. Alternatively, decrease resonance intensity can be due to chemical exchange between

bound and unbound states that can result in line broadening, depending on the affinity and chemical shift change resulting from the interaction. In order to define the minimal epitope sequence recognized by VHH F8-2, an epitope mapping was performed using yeast 2-hybrid with a library of tau fragments as preys (N-terminal GAL4-activation domain fusion,GAL4-AD-tau_fragments), and VHH F8-2 as bait (LexA C-terminal fusion, VHH-LexA fusion). This yeast 2-hybrid screen was possible only because VHH F8-2 was able to bind tau when expressed in the cytoplasm, as demonstrated in a neuroblatoma cell line (**Fig. 4**). 84 positive clones, indicative of VHH F8-2 binding to one tau fragment, were selected from a small-scale cell-to-cell mating screen. The minimal common amino acid sequence in all the corresponding tau fragment prey sequences identified peptide $_{373}$THKLTF$_{378}$ of tau as the epitope of VHH F8-2 (**Fig. S6**). This result is in agreement with the NMR data, the peptide $_{373}$THKLTF$_{378}$ being included in the region $_{370}$KIE**THKLTF**RENAKAKT$_{386}$. It additionally showed that the NMR strength lied in the efficiency to identify regions of binding in a series of VHHs, rather than in the precise delimitation of the epitope.

Affinity optimization of VHH F8-2

Our results have emphasized a diversity of binding affinities displayed by a family of VHHs sharing the same CDR3 loop and the same epitope (**Fig. 1-3**). It suggested the possibility of binding affinity improvement, with or without modification of the CDR3 loop. A strategy of limited random mutagenesis coupled with yeast two-hybrid screening was chosen for affinity optimization in intracellular conditions. A cDNA mutant library was thus first built by random mutagenesis, targeting the whole sequence of VHH F8-2 to produce a variety of VHH preys (N-terminal GAL4-activation domain fusion, GAL4AD-VHH F8-2) against the tau bait (N-terminal LexA fusion, LexA-tau310-383). The library was transformed in yeast and screening of the library was carried out by cell-to-cell mating on selective medium without histidine (His-) and with 200mM 3AT (3-Amino-1,2,4-triazole). The interaction between the bait (LexA-tau310-383) and a prey (GAL4AD-VHH F8-2) was detected by the growth of a diploid yeast colony (auxotrophic for histidine) on the selective medium. Growth is dependent on the transcription of the *his3* reporter gene, which results from interaction between the GAL4-AD and LexA fusion proteins. Mutants of VHH-F8-2 with an improved affinity for tau were

selected on the His- medium by increasing the selection pressure using 3AT (3-amino-1,2,4-triazole), the later compound being a competitive inhibitor of the *his3* reporter gene product, to reach conditions with no detection of interaction for VHH-F8-2 with tau (200mM 3AT). The improved interaction of some selected VHH clones resulting from this primary screen was further confirmed by one-to-one mating assay using full-length tau 0N4R fused to LexA (C-terminal LexA fusion, tau-LexA) as bait. The selectivity of the medium was increased to detect growing colonies in conditions corresponding to undetected VHH F8-2-tau interaction. This selection condition was obtained on a medium without histidine and with 1 mM 3AT (**Fig. 5**). The selection was convergent and identified three VHH F8-2 mutants growing on medium without histidine and with 1 mM or 10mM of 3AT compound (**Fig. 5**). The mutations were located in the framework regions, for mutants F8-2_{S54L} and F8-$2_{S54L+T128A}$, or in the CDR3 loop for F8-2_{R111C} (**Fig. 1**). Conservation of the epitope was confirmed by NMR resonance perturbation mapping, using ^{15}N-tau spectrum to probe the interaction with each of these VHHs (**Fig. S7-S9**).

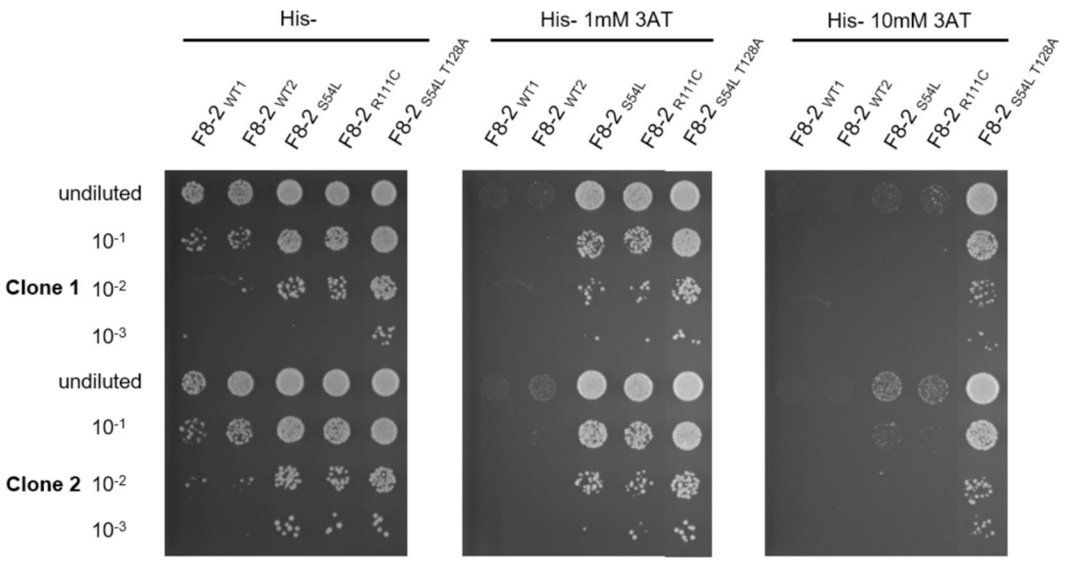
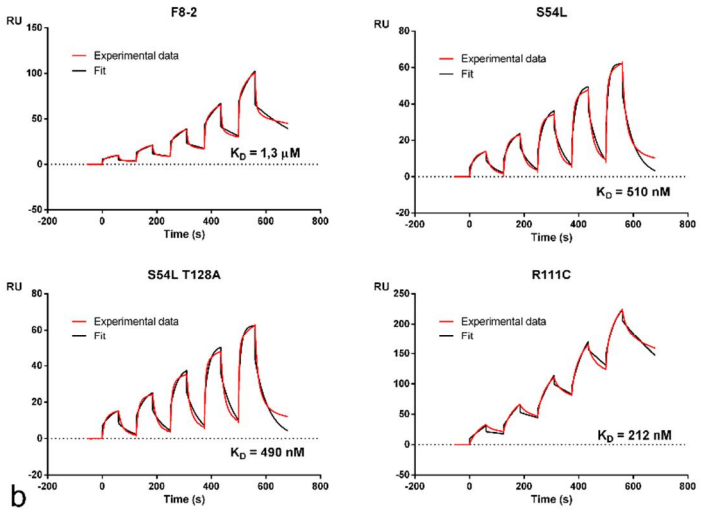


Figure 5: Selection of VHHs F8-2 mutants with an improved binding capacity to tau. Interaction between the bait (tau-LexA) and a prey (GAL4AD-VHH F8-2) was detected by the growth of a diploid yeast colony (auxotrophic for histidine) on the selective medium without histidine (His-). Mutants of VHH-F8-2 with an improved affinity for tau were selected on a His- selective medium by increasing the selection pressure with 1mM or 10mM of 3AT. From 1 mM 3AT concentration, there is no more detection of interaction between VHH-F8-2 (GAL4AD-VHH F8-2) with tau (tau-LexA). Drops of two independent diploid cell cultures are presented.

In particular, a single substitution in the CDR3 loop (F8-2_{R111C}) did not influence epitope recognition. In regard to that observation, the interaction of an antibody with a disordered epitope was proposed to show an asymmetry, in the sense of a sensitivity to modification of the disordered recognition sequence (epitope) but none (or low) to modification in the paratope of the ordered binding partner, the VHH[29].

Interaction of optimized mutants with tau was further characterized using SPR with biotinylated-tau immobilized at the surface of a streptavidin-functionalized chip. The assay provided the kinetic parameters of each optimized VHH-tau interactions, characterized by dissociation constants K_D of 211 nM for VHH F8-2_{R111C}, 507 nM for F8-2_{S54L} and 489 nM for F8-$2_{S54L+T128A}$. (**Fig. 6a-b**). Optimization resulted in a 2- to 6-fold upgrade in affinity confirming the possibility to improve binding affinity using this method and providing new efficient VHHs targeting tau C-terminal domain. The gain in affinity resulting from modification of a single amino acid in the CDR3 loop was important, with a decrease of the K_D from 1332 nM to 211 nM. Interestingly, modification of one amino acid residue in the FR- albeit adjacent to the CDR2 loop - S54L, also provided a gain in affinity. This again emphasized the importance of the CDR1-2 loops in the VHH properties. Of note, the double mutant F8-$2_{S54L+T128A}$ did not show improved affinity compared to the single mutant F8-2_{S54L} in *in vitro* assays (**Fig. 6b**), but proved to have the best intracellular binding capacity in yeast two-hybrid selection, characterized by growth of the corresponding diploid without histidine and with 10mM 3AT (**Fig. 5**). This second mutation in the FR, T128A at the C-terminus of the VHH, might thus not directly influence the interaction, but rather the stability of the VHH in a cellular context. This observation emphasizes a possible change of the VHH properties depending on their expression system that needs to be considered. Were these VHH meant for therapy, for example, gene therapy or passive immunotherapy, this consideration may lead to a different choice of the best suited antibody in the VHH series.

a



b

VHH	k_{on} (1/M.s)	k_{off} (1/s)	K_D (nM)	SE (nM)
F8-2	3170	0,0042	1332	31,3
F8-2_{R111C}	13300	0,0028	211	2
F8-2_{S54L}	43500	0,0220	507	9,8
F8-$2_{S54L\ T128A}$	39400	0,0192	489	11,3

Figure 6: Affinity determination for the optimized VHHs binding tau by SPR. **a.** Sensorgrams obtained by single cycle kinetics method of VHH F8-2 and optimized mutants titrated on immobilized tau. **b.** Table of kinetic and thermodynamic constants. Dissociation equilibrium constant K_D is calculated as the ratio of the off-rate on the on-rate k_{off}/k_{on}. Each single cycle kinetics analysis was performed on immobilized biotinylated tau 2N4R (500 RU), with five injections of VHH analyte at 0.125 µM, 0.25 µM, 0.5 µM, 1 µM, and 2 µM for mutant F8-2 R111C) or 0.25 µM, 0.5 µM, 1 µM, 2 µM and 4 µM (other mutants).

Tau detection using optimized VHH F8-2

VHHs F8-2_{S54L} and F8-2_{R111C} were subsequently used in a conventional immune assay to validate their ability to detect recombinant tau or tau in brain lysates. We chose VHH F8-2_{R111C}, which showed the lowest K_D in the optimization procedure (**Fig. 6b**), for the first assay. F8-2_{R111C} used as primary antibody detected recombinant tau 2N4R or tau 1N4R from transgenic mice THY-Tau30[30] brain lysate (**Fig. 7a**, **Fig. S10a-b**). However, the signal-to-noise ratio was poor (**Fig. S10a-b**), the unspecific signals arising partly from the secondary antibody directed against the VHH (**Fig. S10a-b**). We thus next used minibodies (Mbs) derived from both VHHs F8-$2_{R111C.}$ and F8-2_{S54L}. To this end, the VHHs were fused with the Fc domain of mouse IgG2a, allowing the use of a conventional anti-IgG secondary antibody[31]. The detection of tau by western blot using these Mbs was comparable to the one obtained using the VHHs, but the signal to noise was improved (**Fig. S10d,e**). The use of Mbs may increase the signal-to-noise ratio thanks to an avidity mechanism mediated by multivalent binding; because Mbs are bifunctional binders due to the link of two VHHs to one Fc fragment. However,

neither the VHHs nor the Mbs had enough sensitivity to detect purified insoluble tau from AD brain (**Fig. 7a**, **Fig. S10b-e**). Note that tau in these AD brain extracts was also barely detected by the anti-tau Cter IgG antibody in the conditions of our experiment. These results nevertheless encouraged us to assay F8-2_{R111C}, as a Mb in immunohistochemistry of brain sections from ten months old transgenic THY-Tau30 mice[30]. We performed tau labeling using the anti-tau Cter antibody as a positive control and brain sections from a transgenic KO-tau mouse model as a negative control (**Fig. 7b**, **Fig. S11a,c**). The polyclonal anti-tau Cter and VHH F8-2 antibodies recognize the same tau domain, but not the same epitope. With THY-Tau30 brain sections, a clear signal was observed from the Mb labeling, showing an accumulation of tau in neurons of the CA1 layer from hippocampus. A good overlap with the signal obtained in the same conditions with anti-tau Cter polyclonal antibody was confirmed by merging of the signals (**Fig. 7c**, **Fig. S11b,d**). These experiments demonstrated the ability of F8-2-derived VHHs to bind with specificity their tau target in transgenic mouse brain tissues, in the same manner as an entire IgG.

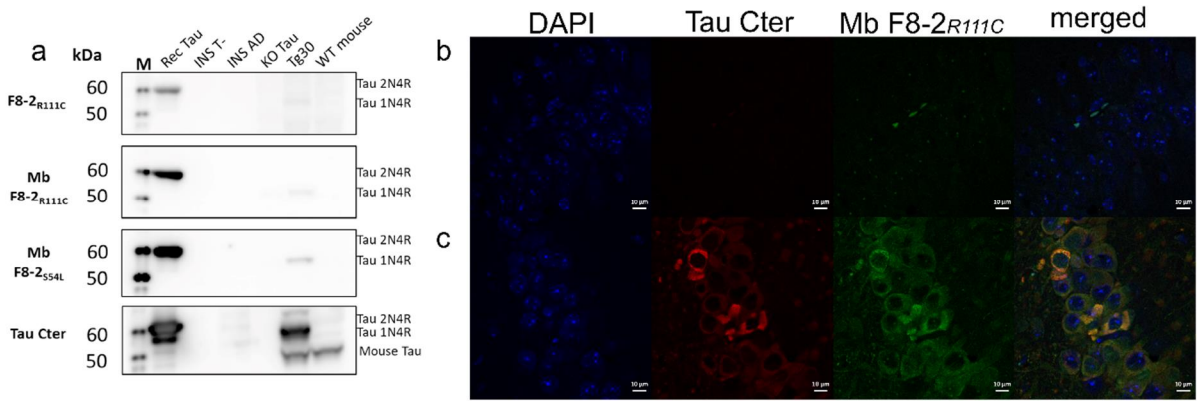


Figure 7: Tau detection in transgenic mouse models by F8-2-derived VHHs. **a.** Western blot analysis of recombinant 2N4R tau (Rec Tau), sarkosyl insoluble fraction from a human control brain (INS T-), sarkosyl insoluble fraction from an AD brain patient (INS AD), brain lysate from transgenic KO-Tau mouse model (KO Tau), from transgenic THY-Tau30 mouse model (Tg30) and wild-type mouse (WT mouse) by VHH F8-2_{R111C} (F8-2_{R111C}), minibody F8-2_{R111C} (Mb F8-2_{R111C}), minibody F8-2_{S54L} (Mb F8-2_{S54L}) and anti-tau Cter polyclonal antibody (Tau Cter). **b**. Immunofluorescence labeling of tau in the CA1 layer of hippocampus from transgenic KO-tau mice revealed by anti-tau Cter and minibody F8-2_{R111C}. **c**. Immunofluorescence labeling of tau in the CA1 layer of hippocampus from transgenic THY-Tau30 mice revealed by anti-tau Cter polyclonal antibody and minibody (Mb) F8-2_{R111C}.

CONCLUSIONS

Tau pathology progression through the various brain regions in AD is strongly associated with cognitive decline[32,33], and tau is consequently an attractive target for therapeutic intervention. Interest for tau immunotherapy has grown in recent years[10,11]. Tau has several domains that might represent target for diverse strategies, depending of the desired effect: blocking aggregation, seeding or slowing tau neuron-to-neuron transfer[34,35]. However, no rule has yet emerged as to the best epitope(s) to consider about mitigation of tau pathology, although a better fundamental knowledge might spare a lot of disappointments in latter clinical stages. Similarly, it is not known whether tau in the cellular compartment or extracellular one might be the best target. VHHs against tau, including the family of VHHs here described, recognizing the C-terminal region of tau protein, represent interesting tools to address these important questions. In addition to their interest to understand tau physiopathology, it was shown that an effector function, provided by the Fc region of the IgG, is not required to reduce accumulation of tau pathology in a P301L-Tg mouse model[36]. The absence of effector function of the VHHs might thus prevent potential inflammatory side effects of immunotherapy while preserving its therapeutic potential. VHHs might consequently represent a safer alternative in tau therapies than the IgG-based approaches.

METHODS

Selection and screening of the VHHs directed against tau protein

Recombinant tau protein was biotinylated using EZ-LinkÊ Sulfo-NHS-Biotin (Thermo Fisher Scientific) using manufacturer conditions except for a two-fold molecular excess of Sulfo-NHS-Biotin. The unreacted Sulfo-NHS-Biotin was eliminated using Prepacked Columns SepadextranÊ 25 Medium SC (Proteigene). The Nali-H1 library of VHHs was screened against the recombinant biotinylated-tau as described previously[23]. Biotinylated-tau protein was bound to DynabeadsÊ M-280 Streptavidin (Invitrogen) at each round of selection, at a concentration gradually decreased: 100nM in first round, 50nM in second round and 10nM in third round. Biotinylated-tau binding was verified by Western Blot using Streptavidin Protein, HRP (Thermo Fisher Scientific). $3x10^{11}$ phages of the Nali-H1 library were used in the first round of selection. After the third round, 186 clones were randomly picked and tested in non-absorbed Phage ELISA assay using avidin-plates and biotinylated-tau

Antigen (5µg/ml) for cross-validation[37]. Selected clones were then cloned into pHEN2 vector as in[23] for recombinant production in bacteria.

Production and purification of the VHHs

Competent *Escherichia coli* BL21(DE3) bacterial cells were transformed with the various PHEN2-VHH constructs. Recombinant *E.coli* cells produced proteins targeted to the periplasm after induction by 1 mM IPTG (isopropylthiogalactoside). Production was pursued for 4 hours at 28°C before centrifugation to collect the cell pellet. Pellet was suspended in 200 mM Tris-HCl, 500 mM sucrose, 0.5 mM EDTA, pH 8 and incubated 30 min on ice. 50 mM Tris-HCl, 125 mM sucrose, 0.125 mM EDTA, pH 8.0 and complete protease inhibitor (Roche) were then added to the cells suspension and incubation continued 30 min on ice. After centrifugation, the supernatant, corresponding to the periplasmic extract, was recovered. The VHHs were purified by immobilized-metal affinity chromatography (HisTrap HP, 1mL, GE healthcare) followed by size exclusion chromatography (Hiload 16/60, Superdex 75, prep grade, GE healthcare) equilibrated in NMR buffer (50 mM NaPi pH 6.7, 30 mM NaCl, 2.5 mM EDTA, 1 mM DTT).

Production and purification of labelled ^{15}N-tau

pET15b-tau recombinant T7 expression plasmid was transformed into competent *E.coli* BL21(DE3) bacterial cells. A small-scale culture was first grown in LB medium at 37 °C and was next added at 1:10 V/V to 1L of a modified M9 medium containing MEM vitamin mix 1X (MilliporeSigma), 4g of glucose, 1g of ^{15}N-NH_4Cl, 0.5g of ^{15}N-ISOGRO (MilliporeSigma), 0.1 mM $CaCl_2$ and 2 mM $MgSO_4$. Recombinant ^{15}N-tau production was induced with 0.5 mM IPTG when the culture reached an OD600 of 0.8. ^{15}N-tau was first purified by heating the bacterial extract 15 min at 75°C. The resulting supernatant was next passed on a cation exchange chromatography column (Hitrap SP sepharose FF, 5mL, GE healthcare) equilibrated in 50 mM sodium phosphate buffer (NaPi) pH 6.5 and eluted with a NaCl gradient. tau pooled fractions were buffer-exchanged in 50 mM ammonium bicarbonate (Hiload 16/60 desalting column, GE Healthcare) for lyophilization[38].

NMR Spectroscopy experiments

Analysis of the ^{15}N-tau/VHH samples was performed at 298K on 900 MHz Bruker Avance NEO spectrometer equipped with a cryoprobe. Tri-methyl silyl propionate was used as internal reference.

Lyophilized ^{15}N-tau was diluted in NMR buffer and mixed with each of the VHH, at 100 µM final concentration for each protein. 200 µL of each mix in 3 mm tubes were sufficient to obtain the 2D ^{1}H, ^{15}N HSQC spectra. ^{1}H, ^{15}N HSQC were acquired with 3072 and 416 points in the direct and indirect dimensions, respectively for 12.6 and 25 ppm, in the ^{1}H and ^{15}N dimensions, respectively, with 32 scans. Data were processed with Bruker Topspin and analyzed with Sparky (T. D. Goddard and D. G. Kneller, SPARKY 3, University of California, San Francisco).

Determination of kinetic and thermodynamic constants by surface plasmon resonance

Affinity measurements were performed on a BIAcore T200 optical biosensor instrument (GE Healthcare). Recombinant tau proteins were biotinylated with 5 molar excess of NHS-biotin conjugates (Thermofisher) during 4 hours at 4°C. On average, 3 biotin molecules were assessed by mass spectrometry to be attached on one tau molecule (Shimadzu Axima Assurance Maldi-Tof mass spectrometer). Capture of biotinylated tau was performed on a streptavidin SA sensorchip in HBS-EP+ buffer (10 mM HEPES, 150 mM NaCl, 3 mM EDTA, 0,05% (v/v) surfactant P20, pH 7.4, GE Healthcare). Biotinylated-tau was injected in flow cell (FC) 2 at a flow-rate of 30 µL/min, until the total amount of captured tau reached 500 resonance units (RUs). tau-functionalized chip allowed screening of all the purified VHHs on FC 2. FC 1 was used to evaluate nonspecific binding and provide background corrections. VHHs were injected sequentially with increased concentrations ranging between 0.125 and 2 µM or 0.25 and 4 µM depending on the VHH, in a single cycle without regeneration of the sensorship between injections. Regeneration consisting in three successive washes of 1 M NaCl was performed between each VHH run. Binding parameters were obtained by fitting the experimental data with the 1:1 Langmuir model of the BIAevaluation sotware. Single-Cycle Kinetics (SCK) analysis was performed to determine the association (k_{on}) and dissociation (k_{off}) kinetic constants, which were used to calculate the thermodynamic equilibrium constants (K_D).

Tau Fragment library construction

Tau cDNA (NM_016834.4) was amplified from lexA bait vector with oligonucleotide oli6690 and oli6972 (**Supplementary information SI 12**) using Phusion polymerase (New England Biolabs, NEB) according to the manufacturerôs protocol and purified using PCR clean up (Macherey-Nagel GMBH). 5 µg of PCR product was next subjected to Fragmentase® treatment according to the manufacturerôs

protocol (NEB). The fragmentation was monitored by migration on agarose gels until a smear around 400-500pb was visible. The fragmented DNA was extracted with phenol/chloroform, recovered by ethanol precipitation and finally subjected to end repair (#E5060S) according to manufacturerôs protocol. dA-tail modification (#E6053S NEB) was next obtained using Blunt/TA Ligase Master Mix with NEBNext® Adaptor hairpin loop (#M0367L, #E7350S NEB) and purification with AMPure XP beads (Beckman Coulter). After USER® enzyme digestion (# M5505S, NEB), the modified DNA was amplified by 15 PCR cycles with NEBNext® Q5® Hot Start HiFi PCR Master Mix (#M0543S) using oligonucleotide oli10829 and oli10830 (**SI 12**). These oligonucleotides were designed to contain Gap Repair recombination sequences to allow recombination into the Gal4 AD prey plasmid pP7. The obtained DNA library included 50 000 independent clones.

Tau fragment library screening

The coding sequence of VHH F8-2 was amplified by PCR and cloned into pB29 as a N-terminal fusion to LexA (VHH F8-2_LexA). The construct was used to produce a bait to screen tau fragment library constructed into pP7. pB29 and pP7 derive from the original pBTM116[39] and pGADGH[40] plasmids, respectively. Tau fragment library was screened using a mating approach with YHGX13 (Y187 ade2-101::loxP-kanMX-loxP, matŬ) and L40ΔGal4 (mata) yeast strains[41]. 84 His+ colonies corresponding to 16000 tested diploids were selected on a medium lacking tryptophan, leucine and histidine. The cDNA from the prey fragments of the positive clones were amplified by PCR and sequenced at their 5ô and 3ô junctions.

Analysis of tau-VHH F8-2 interaction in N2A cells

Stable N2A neuroblastoma cells were plated at a density of 100k cells/well in 24-well plate in 24-well plate (Corning) containing glass-slides coated with poly-D-lysine 0.5 mg/mL and laminin 2 µg/mL and were grown overnight. At 80 % confluency, cells were transfected with the pEM15 plasmid expressing plasma membrane-targeted green fluorescent (GFP) protein[42] fused to tau (GFP-tau) and/or pmCherry plasmid expressing VHH F8-2 fused to the mCherry (VHH F8-2-m-Cherry)[23].

Transfection complexes were obtained by mixing 18.5 µL DMEM medium and 1.5 µL lipofectamine 2000 (Invitrogen) with DMEM medium and 500 ng of plasmid (500 ng of each plasmid for co-transfections) in a total volume of 40 µL per well. Lipoplexes were incubated at room temperature

during 20 min before adding to the cells. Cells were incubated for 24 h with lipoplexes and with 1 mL/well of DMEM medium containing 1% fetal bovine serum. Cells were then washed with pre-warmed PBS and fixed in 4% paraformaldehyde during 20 min. Cells were washed three times with 50 mM NH_4Cl in PBS and incubated with DAPI (1/5000 in PBS) during 10 min. Glass-slides were recovered and treated with DAKO mounting medium (Agilent). Fluorescence data were obtained with a Zeiss confocal microscope using Zeiss Black software.

Affinity optimization of VHH F8-2

VHH F8-2 was amplified from pHEN2 plasmid (oligonucleotides oli3390 and oli3880, supplementary information **SI 13**) using Taq polymerase with 14 mM $MgCl_2$ and 0.2 mM $MnCl_2$ and a modified nucleotide pool[43]. The amplified cDNAs were transformed in yeast Y187 strain, together with a digested empty derivative of pGADGH vector[40], allowing recombination by gap repair into the vector. The VHH cDNAs were expressed as preys, with a N-terminal GAL4-activation domain fusion (GAL4AD-VHH-F8-2). A library of 6 million clones was obtained, collected and aliquoted. Fragment of tau(310-383) isoform 0N4R was expressed as bait with an N-terminal fusion with LexA (LexA-tau(310-383)) from pB27 vector (derived from pBTM116)[39]. The library was screened at saturation, with 14 million tested diploids[41] by increasing the selection pressure with 200mM 3-Amino-1,2,4-Triazol (3AT). The improvement in affinity of some selected clones was confirmed by one-to-one mating assay with L40ΔGal4 (mata) yeast strain transformed with the bait, corresponding to tau variant 0N4R isoform (NM_016834.4) with a C-terminal fusion with LexA (tau-LexA) in pB29 plasmid, and Y187 (matŬ) yeast strain transformed with the prey[41]. Diploïds were grown on selection medium with increasing selection pressure by 3AT from 0 to 10mM.

Production of F8-2-derived minibodies

For expression of dimeric antibodies (minibodies, Mbs), VHH F8-2_{R111} and VHH F8-2_{S54L} coding sequences were inserted in pFuse plasmid (Invivogen). Minibodies production, corresponding to bifunctional VHH F8-2_{R111} or VHH F8-2_{S54L} fused at their C-terminus to the Fc fragment of mouse IgG2, was performed according to Moutel et al.[31]. Briefly, in wells of a 24-well plate, 200000 HEK293 cells were transfected with 0.5 µg DNA using X-tremeGENEÊ (Roche) according to the manufacturer protocol. 24 hours after the transient transfection, the transfection media was exchanged

for a serum-free media, and the cell supernatant collected 5 days later. The presence of the Mbs in this supernatant was confirmed by western blot using an anti-mouse IgG antibody (Jackson).

Western blot analysis

The different samples were loaded onto a 12% Bis-Tris Criterion gel (Biorad), followed by transfer onto a 0.45 mm nitrocellulose membrane, using the Criterion system (Biorad). The membranes were then incubated with 5% milk blocking solution for 45 min at room temperature. The membranes were next incubated overnight at 4°C with VHH F8-2 $_{R111G}$, Mbs F8-2 $_{R111C}$ or F8-2$_{S54L}$ and antibody anti-tau Cter (home-made, epitope corresponds to the last 11 amino acid residues of tau[44]), as primary antibodies. A 1/200 dilution of VHH F8-2 $_{R111C}$ (150 µM stock concentration), 1/100 dilution of supernatant containing Mbs and a 1/10000 dilution of the anti-tau Cter from rabbit serum were applied. The membranes were then washed and incubated for 1 hour with the appropriate secondary antibody, that corresponded to anti-mouse antibody for Mbs (1/50000, Vector Laboratories), anti-rabbit antibody for the anti-tau C-terminal antibody (1/5000, Vector Laboratories) and anti-VHH antibody for the VHH F8-2 $_{R111C}$ (1/10000, Bethyl Laboratories). The signal was visualized using ECL or ECL prime western blotting detection reagents (GE Healthcare).

Immunofluorescence

THY-Tau30 and KO-Tau transgenic mice paraffined saggital sections were permeabilized 45 min in PBS-0.2 % TritonÊ X-100, blocked with a saturation solution of Donkey serum (Sigma) and further incubated overnight at 4°C with mb F8-2 $_{R111C}$ (1/100 dilution of supernatant) and/or anti-tau Cter (1/1000). Anti-tau Cter and Mb labeling were revealed using respectively Alexa Fluor 568 nm donkey anti-rabbit (Invitrogen) and Alexa Fluor 488 nm donkey anti-mouse (Invitrogen) antibodies (1:1000, 1 hour at room temperature). Sections were finally counterstained with 40,6-diamidino-2-phenylindole (DAPI, 300 nM). Black Soudan labeling was performed to lower auto fluorescence. Fluorescence images were obtained with LSM 710 confocal microscope (Zeiss) at 20X and 63X objectives using Zeiss Black software (Zen Lite 2008, Zeiss).

Acknowledgements

We thank Dr Z. Lens and Dr M. Aumercier for their help on the T200 biacore measurements from the Biomolecular interactions analysis platform (PAIB). We also thank M. Tardivel and A. Bongiovanni for their help on the Zeiss confocal microscope, from the Photonic Microscopy Core BioImaging Center (BiCeL). We are grateful to C. Reverdy from Hybrigenics Services for the production of the minibodies. We thank Dr M.C Gallas for providing us the sagittal brain slices in paraffin.

Abbreviations

AD, Alzheimerôs disease; CDR, complementary determining region; ELISA, enzyme-linked immunosorbent assay; FC, flow cell; FR, framework; HSQC, heteronuclear single quantum correlation; IgG, immunoglobulin G; Mb, minibody; NFT, neurofibrillary tangle; NMR, nuclear magnetic resonance; PHF, paired helical filament; RU, resonance unit; ScFv, single chain variable fragment; SPR, surface plasmon resonance; VHH, variable domain of the heavy-chain only antibodies.

Funding

This study was supported by grants from the LabEx (Laboratory of Excellence, ANR-11-LABX-01) DISTALZ (Development of Innovative Strategies for a Transdisciplinary approach to Alzheimerôs disease), from the ANR ToNIC (ANR-18-CE44-0016-01) and the TUNABLE project from the I-SITE ULNE SUSTAIN program. Our laboratories are also supported by LiCEND (Lille Centre of Excellence in Neurodegenerative Disorders).

The NMR facilities were funded by the Nord Region Council, CNRS, Institut Pasteur de Lille, European Community (FEDER), French Research Ministry and Univ. Lille. We acknowledge support from TGE RMN THC (FR-3050, France) and FRABio (Univ. Lille, CNRS, FR 3688).

Conflict of interest

Arrial A. and Rain J.C. are employees of Hybrigenic services.

Author contributions

E. D., C. D., A. A. performed the experiments and treated the data F.-X. C. recorded the NMR spectra, H. M. prepared recombinant proteins, M. H. performed the IHC experiments, M. C., X. H. supervised the experiments, M.C., X.H., J.-C. R., L.B. revised the manuscript, E.D., C.D., I.L. wrote the

manuscript, all authors read and approved the manuscript, J.-C. R., L. B., I. L. initiated and coordinated the research project

Supporting information

Fig. S1-5 and Fig S7-9 Tau 2D HSQC NMR experiments used to identify VHH epitopes, Fig. S6 Tau fragments multiple sequence alignment to identify F8-2 epitope, Fig. S10 Western blot analysis Fig S11 Immuno-labeling of Tau in neurons of transgenic mice hypoccampus tissues

SI 12 and SI 13 oligonucleotide sequences used for PCR amplification

REFERENCES

(1) Weingarten, M. D.; Lockwood, A. H.; Hwo, S. Y.; Kirschner, M. W. A Protein Factor Essential for Microtubule Assembly. *Proc. Natl. Acad. Sci. U. S. A.* **1975**, *72* (5), 1858–1862.

(2) Sotiropoulos, I.; Galas, M.-C.; Silva, J. M.; Skoulakis, E.; Wegmann, S.; Maina, M. B.; Blum, D.; Sayas, C. L.; Mandelkow, E.-M.; Mandelkow, E.; et al. Atypical, Non-Standard Functions of the Microtubule Associated Tau Protein. *Acta Neuropathol. Commun.* **2017**, *5*, 91. https://doi.org/10.1186/s40478-017-0489-6.

(3) Goedert, M.; Jakes, R. Expression of Separate Isoforms of Human Tau Protein: Correlation with the Tau Pattern in Brain and Effects on Tubulin Polymerization. *EMBO J.* **1990**, *9* (13), 4225–4230.

(4) Brion, J. P.; Flament-Durand, J.; Dustin, P. Alzheimer's Disease and Tau Proteins. *Lancet* **1986**, *2* (8515), 1098. https://doi.org/S0140-6736(86)90495-2 [pii].

(5) Grundke-Iqbal, I.; Iqbal, K.; Quinlan, M.; Tung, Y. C.; Zaidi, M. S.; Wisniewski, H. M. Microtubule-Associated Protein Tau. A Component of Alzheimer Paired Helical Filaments. *J Biol Chem* **1986**, *261*, 6084–6089.

(6) Falcon, B.; Zhang, W.; Murzin, A. G.; Murshudov, G.; Garringer, H. J.; Vidal, R.; Crowther, R. A.; Ghetti, B.; Scheres, S. H. W.; Goedert, M. Structures of Filaments from Pick's Disease Reveal a Novel Tau Protein Fold. *Nature* **2018**, 1. https://doi.org/10.1038/s41586-018-0454-y.

(7) Fitzpatrick, A. W. P.; Falcon, B.; He, S.; Murzin, A. G.; Murshudov, G.; Garringer, H. J.; Crowther, R. A.; Ghetti, B.; Goedert, M.; Scheres, S. H. W. Cryo-EM Structures of Tau Filaments from Alzheimer's Disease. *Nature* **2017**. https://doi.org/10.1038/nature23002.

(8) Mudher, A.; Colin, M.; Dujardin, S.; Medina, M.; Dewachter, I.; Naini, S. M. A.; Mandelkow, E.-M.; Mandelkow, E.; Buée, L.; Goedert, M.; et al. What Is the Evidence That Tau Pathology Spreads through Prion-like Propagation? *Acta Neuropathol. Commun.* **2017**, *5*. https://doi.org/10.1186/s40478-017-0488-7.

(9) Fichou, Y.; Al-Hilaly, Y. K.; Devred, F.; Smet-Nocca, C.; Tsvetkov, P. O.; Verelst, J.; Winderickx, J.; Geukens, N.; Vanmechelen, E.; Perrotin, A.; et al. The Elusive Tau Molecular Structures: Can We Translate the Recent Breakthroughs into New Targets for Intervention? *Acta Neuropathol. Commun.* **2019**, *7* (1), 31. https://doi.org/10.1186/s40478-019-0682-x.

(10) Congdon, E. E.; Sigurdsson, E. M. Tau-Targeting Therapies for Alzheimer Disease. *Nat. Rev. Neurol.* **2018**, *14* (7), 399–415. https://doi.org/10.1038/s41582-018-0013-z.

(11) Jadhav, S.; Avila, J.; Schöll, M.; Kovacs, G. G.; Kövari, E.; Skrabana, R.; Evans, L. D.; Kontsekova, E.; Malawska, B.; de Silva, R.; et al. A Walk through Tau Therapeutic Strategies. *Acta Neuropathol. Commun.* **2019**, *7* (1), 22. https://doi.org/10.1186/s40478-019-0664-z.

(12) Asuni, A. A.; Boutajangout, A.; Quartermain, D.; Sigurdsson, E. M. Immunotherapy Targeting Pathological Tau Conformers in a Tangle Mouse Model Reduces Brain Pathology with Associated Functional Improvements. *J. Neurosci. Off. J. Soc. Neurosci.* **2007**, *27* (34), 9115–9129. https://doi.org/10.1523/JNEUROSCI.2361-07.2007.

(13) Boutajangout, A.; Quartermain, D.; Sigurdsson, E. M. Immunotherapy Targeting Pathological Tau Prevents Cognitive Decline in a New Tangle Mouse Model. *J. Neurosci. Off. J. Soc. Neurosci.* **2010**, *30* (49), 16559–16566. https://doi.org/10.1523/JNEUROSCI.4363-10.2010.

(14) Dai, C.-L.; Tung, Y. C.; Liu, F.; Gong, C.-X.; Iqbal, K. Tau Passive Immunization Inhibits Not Only Tau but Also Aβ Pathology. *Alzheimers Res. Ther.* **2017**, *9* (1), 1. https://doi.org/10.1186/s13195-016-0227-5.

(15) Troquier, L.; Caillierez, R.; Burnouf, S.; Fernandez-Gomez, F. J.; Grosjean, M.-E.; Zommer, N.; Sergeant, N.; Schraen-Maschke, S.; Blum, D.; Buee, L. Targeting Phospho-Ser422 by Active Tau Immunotherapy in the THYTau22 Mouse Model: A Suitable Therapeutic Approach. *Curr. Alzheimer Res.* **2012**, *9* (4), 397–405.

(16) Ising, C.; Gallardo, G.; Leyns, C. E. G.; Wong, C. H.; Stewart, F.; Koscal, L. J.; Roh, J.; Robinson, G. O.; Remolina Serrano, J.; Holtzman, D. M. AAV-Mediated Expression of Anti-Tau ScFvs

Decreases Tau Accumulation in a Mouse Model of Tauopathy. *J. Exp. Med.* **2017**, *214* (5), 1227–1238. https://doi.org/10.1084/jem.20162125.

(17) Spencer, B.; Brüschweiler, S.; Sealey-Cardona, M.; Rockenstein, E.; Adame, A.; Florio, J.; Mante, M.; Trinh, I.; Rissman, R. A.; Konrat, R.; et al. Selective Targeting of 3 Repeat Tau with Brain Penetrating Single Chain Antibodies for the Treatment of Neurodegenerative Disorders. *Acta Neuropathol. (Berl.)* **2018**, *136* (1), 69–87. https://doi.org/10.1007/s00401-018-1869-0.

(18) Hamers-Casterman, C.; Atarhouch, T.; Muyldermans, S.; Robinson, G.; Hamers, C.; Songa, E. B.; Bendahman, N.; Hamers, R. Naturally Occurring Antibodies Devoid of Light Chains. *Nature* **1993**, *363* (6428), 446–448. https://doi.org/10.1038/363446a0.

(19) Muyldermans, S.; Cambillau, C.; Wyns, L. Recognition of Antigens by Single-Domain Antibody Fragments: The Superfluous Luxury of Paired Domains. *Trends Biochem. Sci.* **2001**, *26* (4), 230–235.

(20) Herce, H. D.; Schumacher, D.; Schneider, A. F. L.; Ludwig, A. K.; Mann, F. A.; Fillies, M.; Kasper, M.-A.; Reinke, S.; Krause, E.; Leonhardt, H.; et al. Cell-Permeable Nanobodies for Targeted Immunolabelling and Antigen Manipulation in Living Cells. *Nat. Chem.* **2017**, *9* (8), 762–771. https://doi.org/10.1038/nchem.2811.

(21) Li, T.; Bourgeois, J.-P.; Celli, S.; Glacial, F.; Le Sourd, A.-M.; Mecheri, S.; Weksler, B.; Romero, I.; Couraud, P.-O.; Rougeon, F.; et al. Cell-Penetrating Anti-GFAP VHH and Corresponding Fluorescent Fusion Protein VHH-GFP Spontaneously Cross the Blood-Brain Barrier and Specifically Recognize Astrocytes: Application to Brain Imaging. *FASEB J. Off. Publ. Fed. Am. Soc. Exp. Biol.* **2012**, *26* (10), 3969–3979. https://doi.org/10.1096/fj.11-201384.

(22) Li, T.; Vandesquille, M.; Koukouli, F.; Dudeffant, C.; Youssef, I.; Lenormand, P.; Ganneau, C.; Maskos, U.; Czech, C.; Grueninger, F.; et al. Camelid Single-Domain Antibodies: A Versatile Tool for in Vivo Imaging of Extracellular and Intracellular Brain Targets. *J. Control. Release Off. J. Control. Release Soc.* **2016**, *243*, 1–10. https://doi.org/10.1016/j.jconrel.2016.09.019.

(23) Moutel, S.; Bery, N.; Bernard, V.; Keller, L.; Lemesre, E.; de Marco, A.; Ligat, L.; Rain, J.-C.; Favre, G.; Olichon, A.; et al. NaLi-H1: A Universal Synthetic Library of Humanized Nanobodies Providing Highly Functional Antibodies and Intrabodies. *eLife* **2016**, *5*. https://doi.org/10.7554/eLife.16228.

(24) Lippens, G.; Wieruszeski, J. M.; Leroy, A.; Smet, C.; Sillen, A.; Buee, L.; Landrieu, I. Proline-Directed Random-Coil Chemical Shift Values as a Tool for the NMR Assignment of the Tau Phosphorylation Sites. *Chembiochem* **2004**, *5* (1), 73–78. https://doi.org/10.1002/cbic.200300763.

(25) Mukrasch, M. D.; Bibow, S.; Korukottu, J.; Jeganathan, S.; Biernat, J.; Griesinger, C.; Mandelkow, E.; Zweckstetter, M. Structural Polymorphism of 441-Residue Tau at Single Residue Resolution. *PLoS Biol* **2009**, *7* (2), e34. https://doi.org/doi: 10.1371/journal.pbio.1000034.

(26) Jeganathan, S.; von Bergen, M.; Brutlach, H.; Steinhoff, H. J.; Mandelkow, E. Global Hairpin Folding of Tau in Solution. *Biochemistry* **2006**, *45* (7), 2283–2293. https://doi.org/10.1021/bi0521543.

(27) De Genst, E. J.; Guilliams, T.; Wellens, J.; O'Day, E. M.; Waudby, C. A.; Meehan, S.; Dumoulin, M.; Hsu, S.-T. D.; Cremades, N.; Verschueren, K. H. G.; et al. Structure and Properties of a Complex of α-Synuclein and a Single-Domain Camelid Antibody. *J. Mol. Biol.* **2010**, *402* (2), 326–343. https://doi.org/10.1016/j.jmb.2010.07.001.

(28) Lutje Hulsik, D.; Liu, Y.; Strokappe, N. M.; Battella, S.; El Khattabi, M.; McCoy, L. E.; Sabin, C.; Hinz, A.; Hock, M.; Macheboeuf, P.; et al. A Gp41 MPER-Specific Llama VHH Requires a Hydrophobic CDR3 for Neutralization but Not for Antigen Recognition. *PLoS Pathog.* **2013**, *9* (3), e1003202. https://doi.org/10.1371/journal.ppat.1003202.

(29) MacRaild, C. A.; Richards, J. S.; Anders, R. F.; Norton, R. S. Antibody Recognition of Disordered Antigens. *Struct. Lond. Engl. 1993* **2016**, *24* (1), 148–157. https://doi.org/10.1016/j.str.2015.10.028.

(30) Leroy, K.; Bretteville, A.; Schindowski, K.; Gilissen, E.; Authelet, M.; De Decker, R.; Yilmaz, Z.; Buée, L.; Brion, J.-P. Early Axonopathy Preceding Neurofibrillary Tangles in Mutant Tau Transgenic Mice. *Am. J. Pathol.* **2007**, *171* (3), 976–992. https://doi.org/10.2353/ajpath.2007.070345.

(31) Moutel, S.; El Marjou, A.; Vielemeyer, O.; Nizak, C.; Benaroch, P.; Dübel, S.; Perez, F. A Multi-Fc-Species System for Recombinant Antibody Production. *BMC Biotechnol.* **2009**, *9*, 14. https://doi.org/10.1186/1472-6750-9-14.

(32) Braak, H.; Braak, E. Neuropathological Stageing of Alzheimer-Related Changes. *Acta Neuropathol* **1991**, *82* (4), 239–259.

(33) Hanseeuw, B. J.; Mormino, B. C.; Becker, A.; Sepulcre, J.; Papp, K. V.; Schultz, A. P.; Jacobs, H. IL.; Cosio, D. M.; Chhatwal, J. P.; Sperling, R. A.; et al. Longitudinal Tau Accumulation Is Associated with Cognitive Decline in Normal Elderly. *Alzheimers Dement. J. Alzheimers Assoc.* **2017**, *13* (7), P134–P136. https://doi.org/10.1016/j.jalz.2017.06.2556.

(34) Nobuhara, C. K.; DeVos, S. L.; Commins, C.; Wegmann, S.; Moore, B. D.; Roe, A. D.; Costantino, I.; Frosch, M. P.; Pitstick, R.; Carlson, G. A.; et al. Tau Antibody Targeting Pathological Species Blocks Neuronal Uptake and Interneuron Propagation of Tau in Vitro. *Am. J. Pathol.* **2017**, *187* (6), 1399–1412. https://doi.org/10.1016/j.ajpath.2017.01.022.

(35) Albert, M.; Mairet-Coello, G.; Danis, C.; Lieger, S.; Caillierez, R.; Carrier, S.; Skrobala, E.; Landrieu, I.; Michel, A.; Schmitt, M.; et al. Prevention of Tau Seeding and Propagation by Immunotherapy with a Central Tau Epitope Antibody. *Brain* **2019**, *in press*.

(36) Lee, S.-H.; Le Pichon, C. E.; Adolfsson, O.; Gafner, V.; Pihlgren, M.; Lin, H.; Solanoy, H.; Brendza, R.; Ngu, H.; Foreman, O.; et al. Antibody-Mediated Targeting of Tau In Vivo Does Not Require Effector Function and Microglial Engagement. *Cell Rep.* **2016**, *16* (6), 1690–1700. https://doi.org/10.1016/j.celrep.2016.06.099.

(37) Matz, J.; Chames, P. Phage Display and Selections on Purified Antigens. *Methods Mol. Biol. Clifton NJ* **2012**, *907*, 213–224. https://doi.org/10.1007/978-1-61779-974-7_11.

(38) Danis, C.; Despres, C.; Bessa, L. M.; Malki, I.; Merzougui, H.; Huvent, I.; Qi, H.; Lippens, G.; Cantrelle, F.-X.; Schneider, R.; et al. Nuclear Magnetic Resonance Spectroscopy for the Identification of Multiple Phosphorylations of Intrinsically Disordered Proteins. *J. Vis. Exp. JoVE* **2016**, No. 118. https://doi.org/10.3791/55001.

(39) Vojtek, A. B.; Hollenberg, S. M. Ras-Raf Interaction: Two-Hybrid Analysis. *Methods Enzymol.* **1995**, *255*, 331–342.

(40) Bartel P.L; Sternglanz R. Cellular Interactions in Development: A Practical Approach. In *Cellular interactions in development: A practical approach*; Hartley D.A, Ed.; Practical approach series; 1993; pp 153–179.

(41) Fromont-Racine, M.; Rain, J. C.; Legrain, P. Toward a Functional Analysis of the Yeast Genome through Exhaustive Two-Hybrid Screens. *Nat. Genet.* **1997**, *16* (3), 277–282. https://doi.org/10.1038/ng0797-277.

(42) Skene, J. H.; Virág, I. Posttranslational Membrane Attachment and Dynamic Fatty Acylation of a Neuronal Growth Cone Protein, GAP-43. *J. Cell Biol.* **1989**, *108* (2), 613–624.

(43) Cadwell, R. C.; Joyce, G. F. Randomization of Genes by PCR Mutagenesis. *PCR Methods Appl.* **1992**, *2* (1), 28–33.

(44) Laurent, C.; Dorothée, G.; Hunot, S.; Martin, E.; Monnet, Y.; Duchamp, M.; Dong, Y.; Légeron, F.-P.; Leboucher, A.; Burnouf, S.; et al. Hippocampal T Cell Infiltration Promotes Neuroinflammation and Cognitive Decline in a Mouse Model of Tauopathy. *Brain J. Neurol.* **2017**, *140* (1), 184–200. https://doi.org/10.1093/brain/aww270.

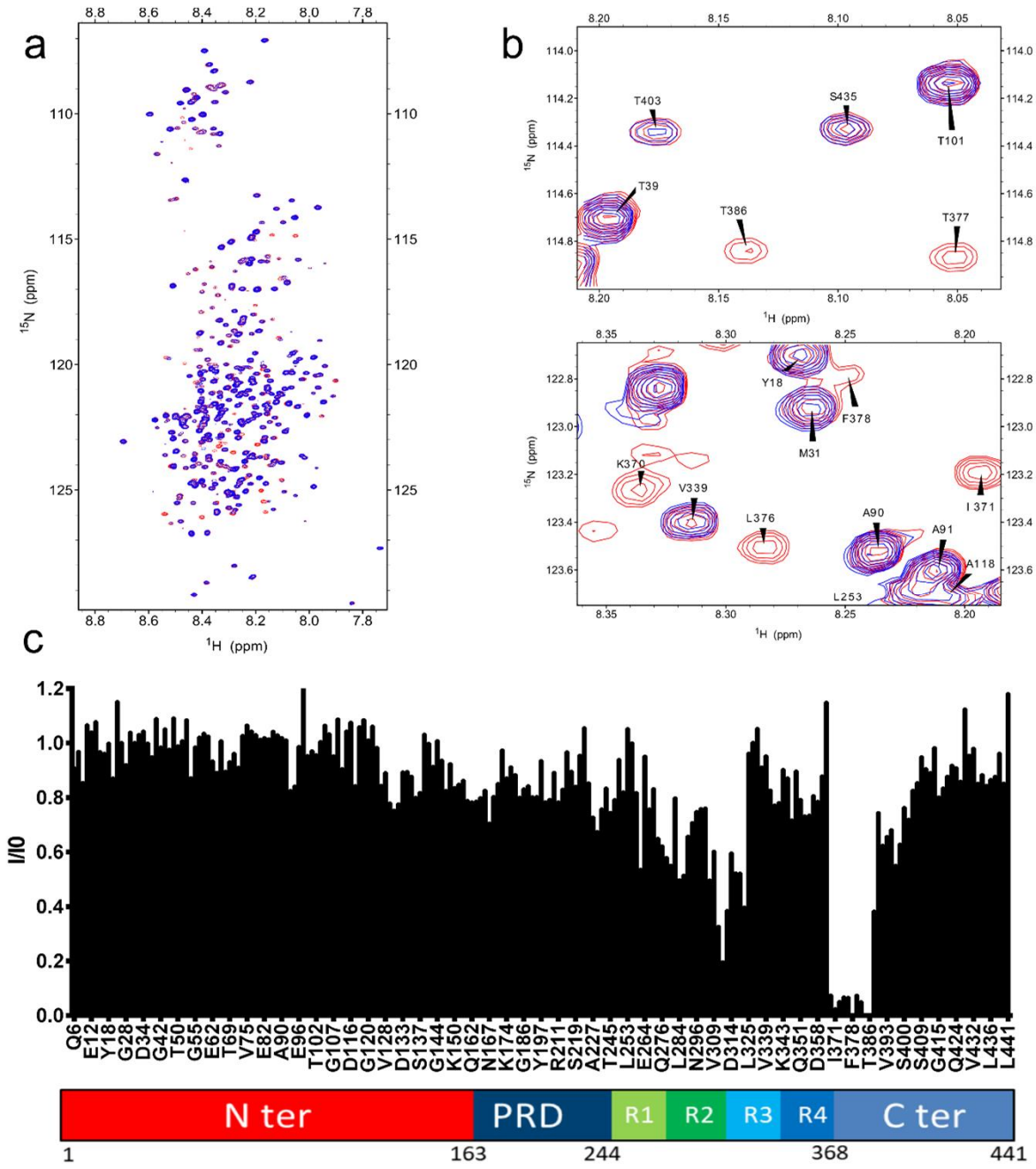


Fig. S1 : Identification of B10-2 epitope using 2D HSQC NMR experiment.

a. Superimposition of two-dimensional ^{1}H, ^{15}N HSQC spectra of ^{15}N-tau (in red) with ^{15}N-tau mixed with non-labelled VHH B10-2 (overlaid in blue). **b.** Spectra enlargements show broadened resonances corresponding to residues implicated in the interaction

c. Normalized intensities I/I0 of corresponding resonances in the two-dimensional spectra of tau with equimolar quantity of VHH B10-2 (I) or free in solution (I0) for residues along the tau sequence. Overlapping resonances are not considered (x-axis is not scaled).

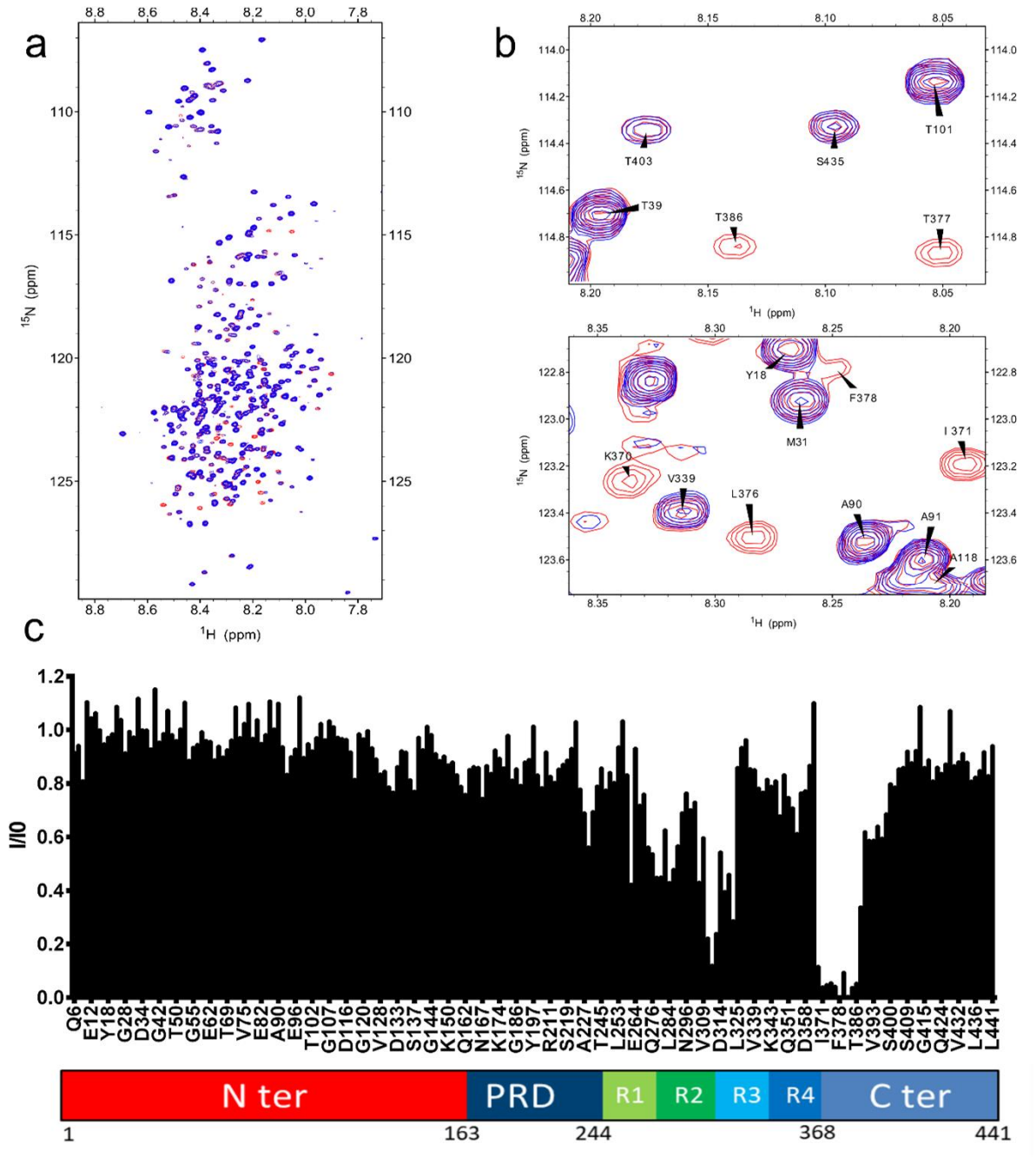


Fig. S2 : Identification of D4-2 epitope using 2D HSQC NMR experiment.

a. Superimposition of two-dimensional ^{1}H, ^{15}N HSQC spectra of ^{15}N-tau (in red) with ^{15}N-tau mixed with non-labelled VHH D4-2 (overlaid in blue). **b.** Spectra enlargements show broadened resonances corresponding to residues implicated in the interaction

c. Normalized intensities I/I0 of corresponding resonances in the two-dimensional spectra of tau with equimolar quantity of VHH D4-2 (I) or free in solution (I0) for residues along the tau sequence. Overlapping resonances are not considered (x-axis is not scaled).

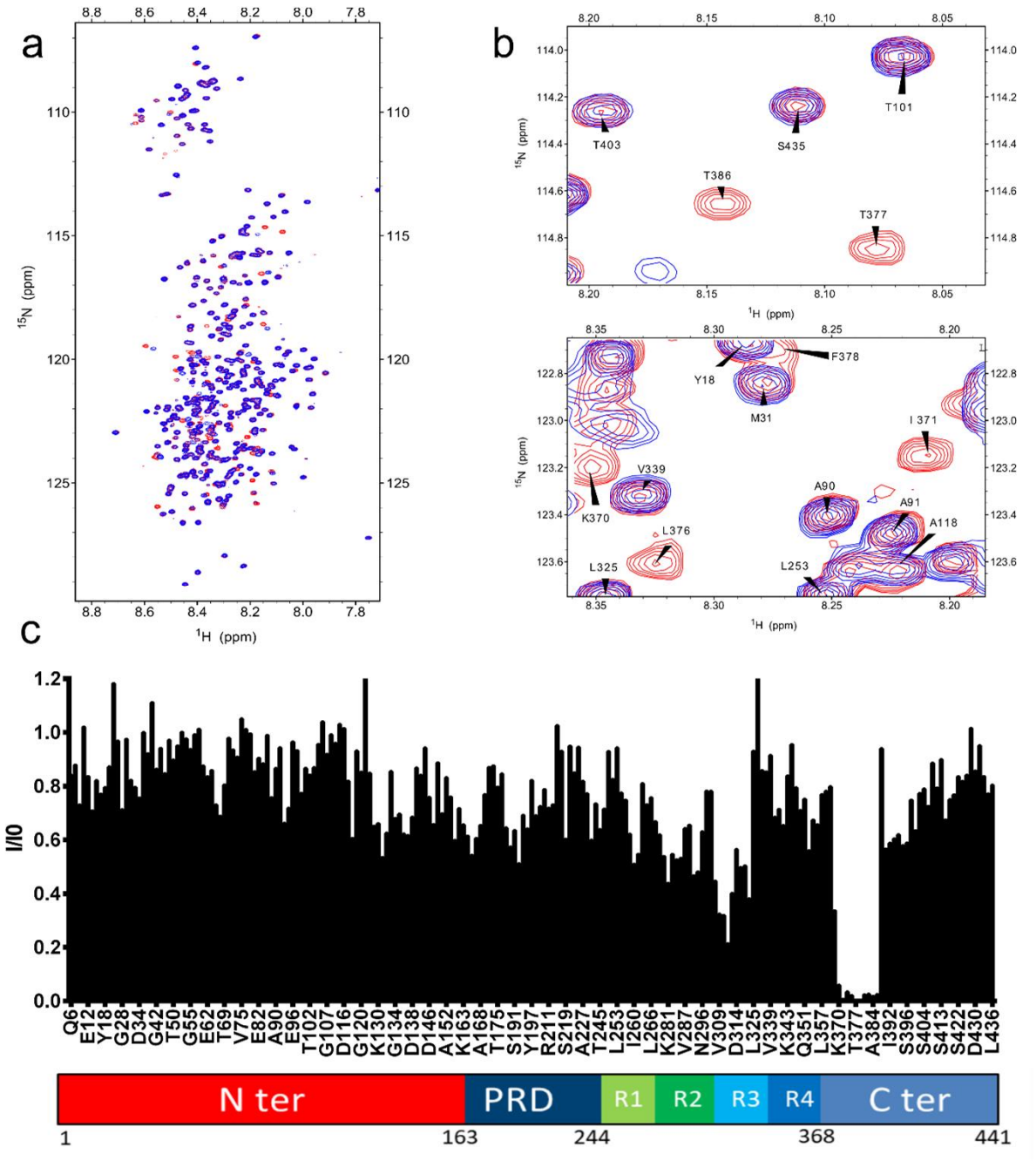


Fig. S3 : Identification of H4-2 epitope using 2D HSQC NMR experiment.

a. Superimposition of two-dimensional ^{1}H, ^{15}N HSQC spectra of ^{15}N-tau (in red) with ^{15}N-tau mixed with non-labelled VHH H4-2 (overlaid in blue). **b.** Spectra enlargements show broadened resonances corresponding to residues implicated in the interaction

c. Normalized intensities I/I0 of corresponding resonances in the two-dimensional spectra of tau with equimolar quantity of VHH H4-2 (I) or free in solution (I0) for residues along the tau sequence. Overlapping resonances are not considered (x-axis is not scaled).

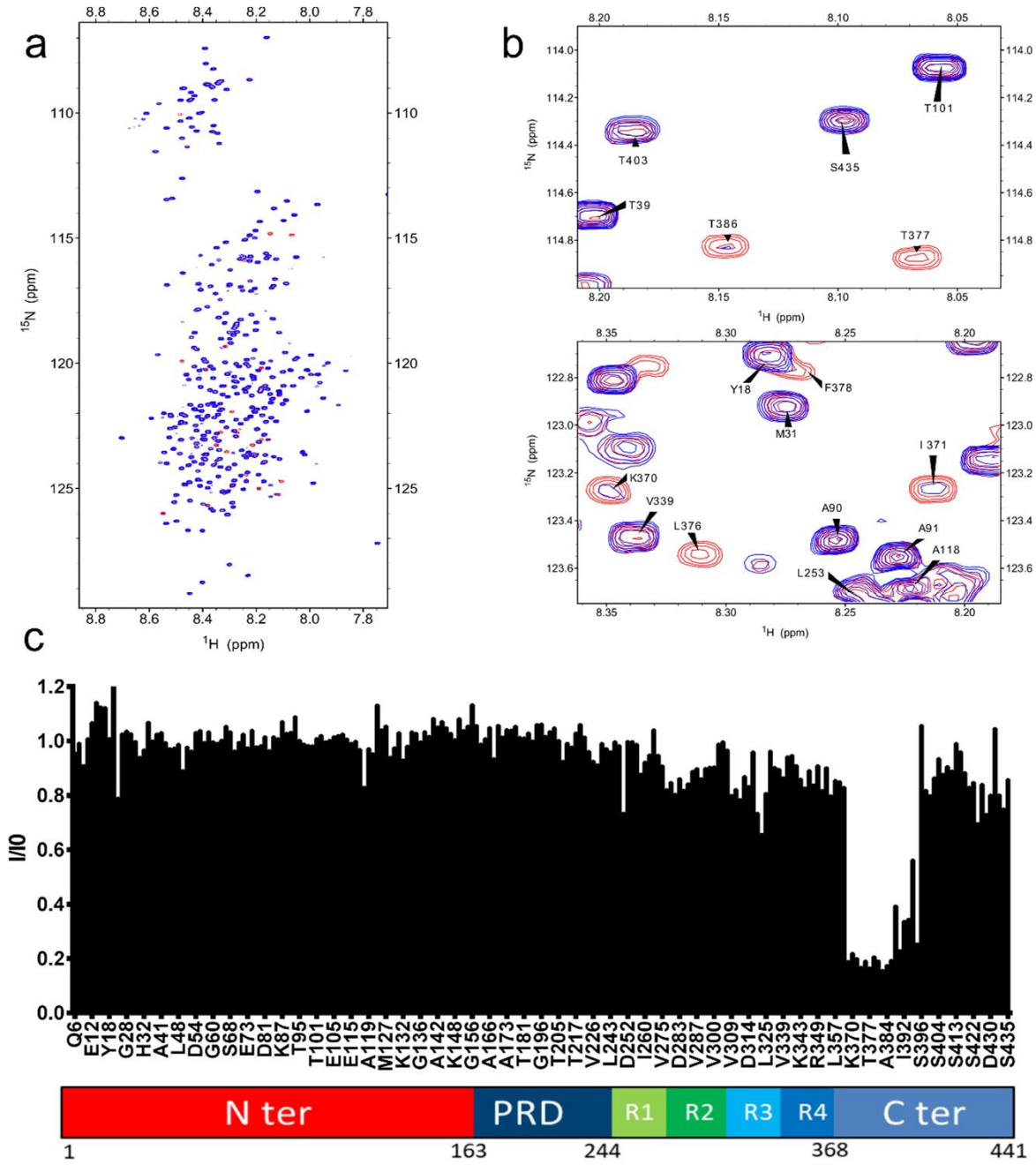


Fig.S4 : Identification of C9-2 epitope using 2D HSQC NMR experiment.

a. Superimposition of two-dimensional ^{1}H, ^{15}N HSQC spectra of ^{15}N-tau (in red) with ^{15}N-tau mixed with non-labelled VHH C9-2 (overlaid in blue). **b.** Spectra enlargements show broadened resonances corresponding to residues implicated in the interaction

c. Normalized intensities I/I0 of corresponding resonances in the two-dimensional spectra of tau with equimolar quantity of VHH C9-2 (I) or free in solution (I0) for residues along the tau sequence. Overlapping resonances are not considered (x-axis is not scaled).

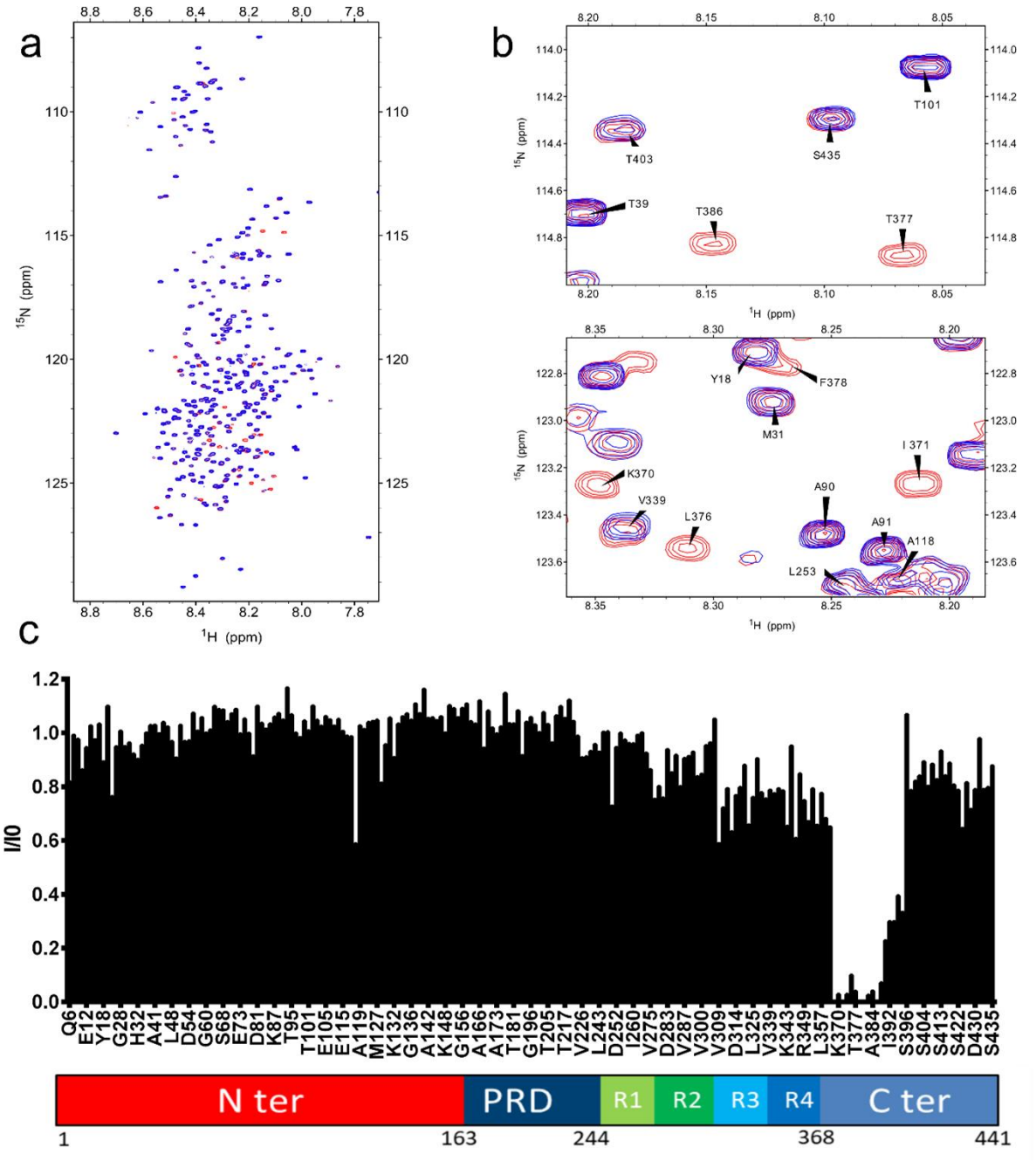


Fig. S5 : Identification of E12-1 epitope using 2D HSQC NMR experiment.

a. Superimposition of two-dimensional ^{1}H, ^{15}N HSQC spectra of ^{15}N-tau (in red) with ^{15}N-tau mixed with non-labelled VHH E12-1 (overlaid in blue). **b.** Spectra enlargements show broadened resonances corresponding to residues implicated in the interaction

c. Normalized intensities I/I0 of corresponding resonances in the two-dimensional spectra of tau with equimolar quantity of VHH E12-1 (I) or free in solution (I0) for residues along the tau sequence. Overlapping resonances are not considered (x-axis is not scaled).

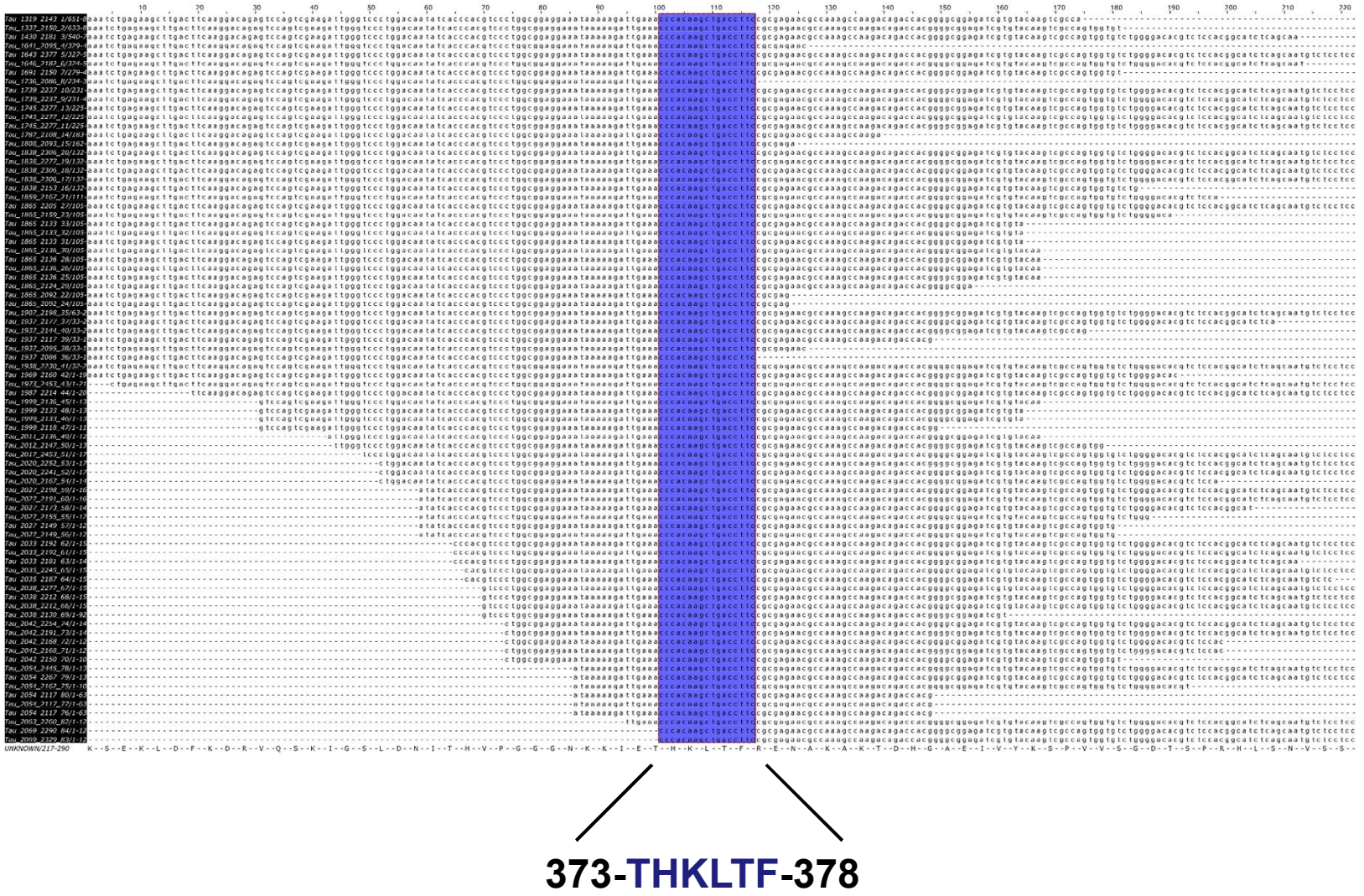


Fig. S6 : Identification of the minimal epitope recognized by VHH F8-2 using tau fragment library and yeast two hybrid. Sequence alignment of the tau fragment sequences corresponding to the 84 positive binders to VHH F8-2. The minimal common sequence is highlighted in blue and corresponds to VHH-F8-2 epitope.

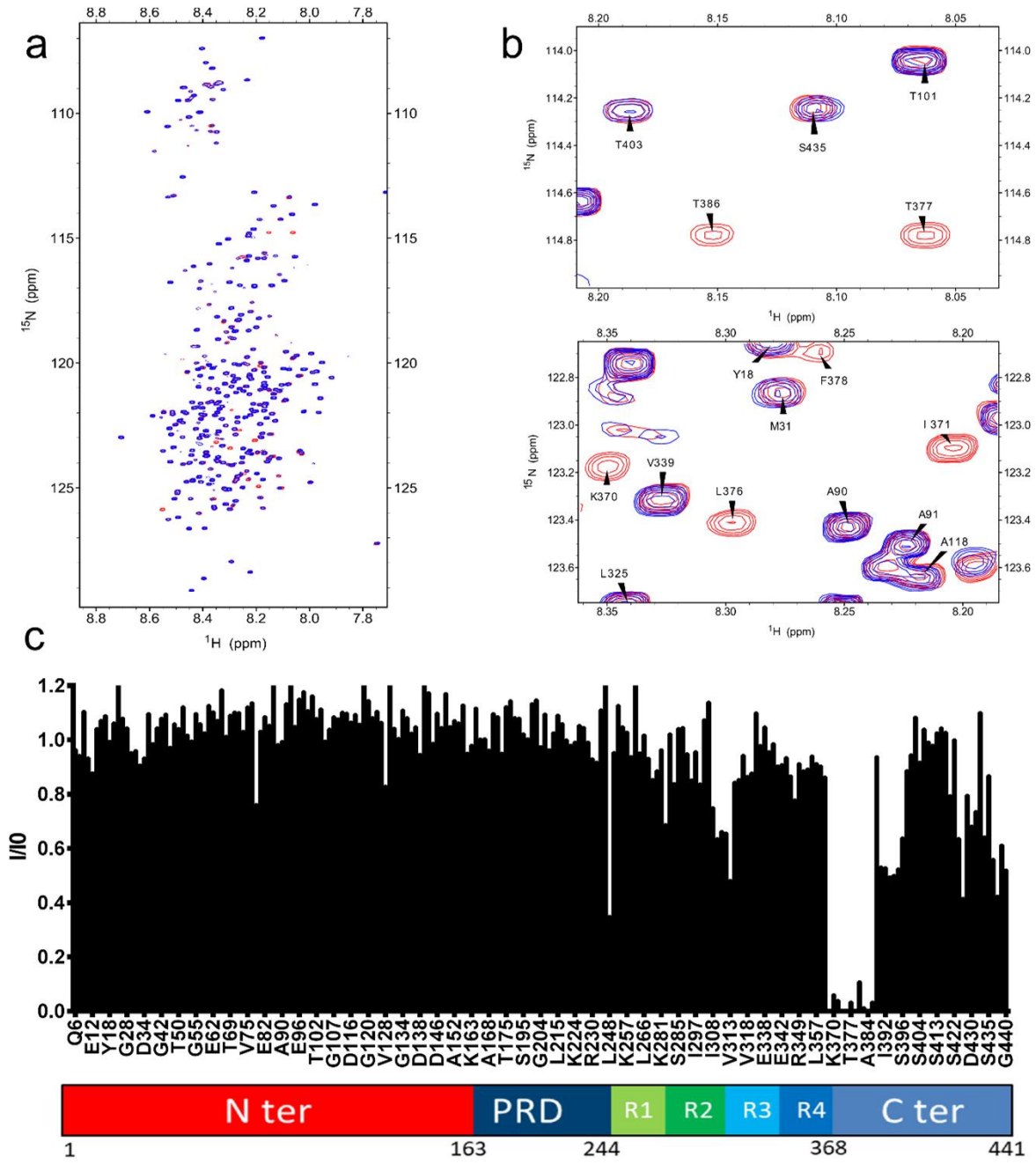


Fig. S7 : Identification of F8-2_{S54L} epitope using 2D HSQC NMR experiment.

a. Superimposition of two-dimensional ^{1}H, ^{15}N HSQC spectra of ^{15}N-tau (in red) with ^{15}N-tau mixed with non-labelled VHH F8-2_{S54L} (overlaid in blue). **b.** Spectra enlargements show broadened resonances corresponding to residues implicated in the interaction

c. Normalized intensities I/I0 of corresponding resonances in the two-dimensional spectra of tau with equimolar quantity of VHH F8-2_{S54L} (I) or free in solution (I0) for residues along the tau sequence. Overlapping resonances are not considered (x-axis is not scaled).

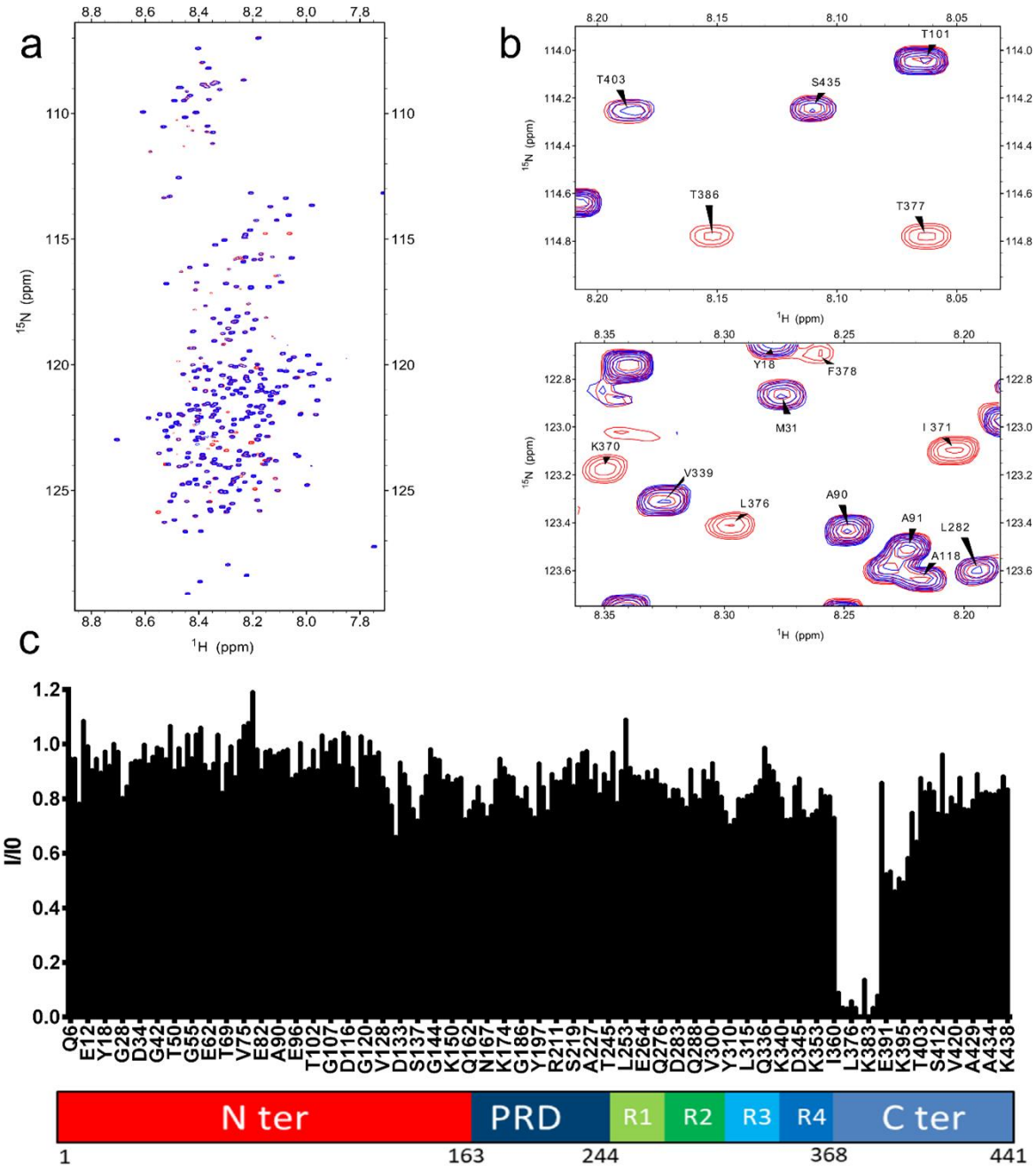


Fig. S8 : Identification of F8-2_{R111C} epitope using 2D HSQC NMR experiment.

a. Superimposition of two-dimensional ^{1}H, ^{15}N HSQC spectra of ^{15}N-tau (in red) with ^{15}N-tau mixed with non-labelled VHH F8-2_{R111C} (overlaid in blue). **b.** Spectra enlargements show broadened resonances corresponding to residues implicated in the interaction

c. Normalized intensities I/I0 of corresponding resonances in the two-dimensional spectra of tau with equimolar quantity of VHH F8-2_{R111C} (I) or free in solution (I0) for residues along the tau sequence. Overlapping resonances are not considered (x-axis is not scaled).

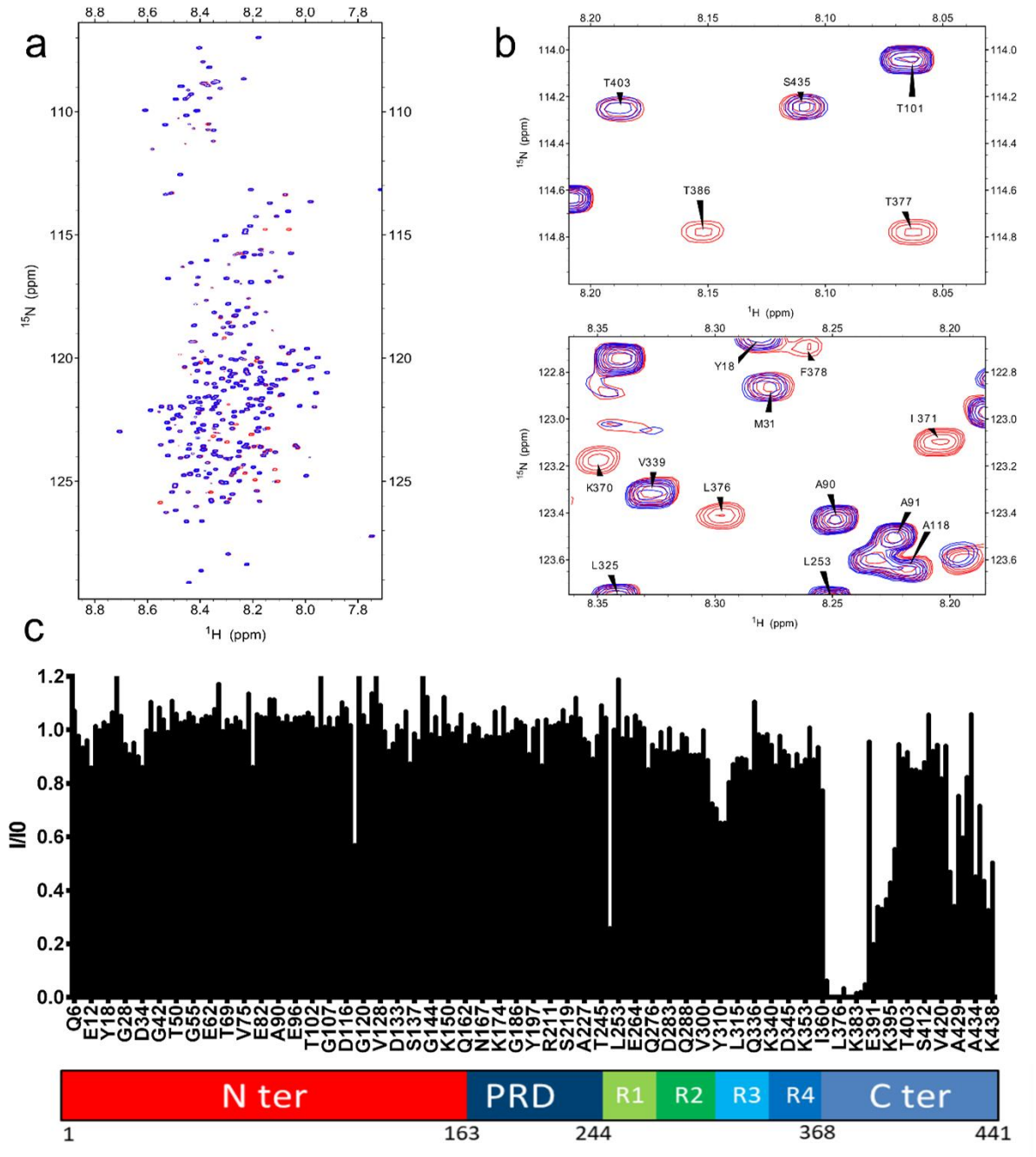


Fig. S9 : Identification of F8-$2_{S54L\ T128A}$ epitope using 2D HSQC NMR experiment.

a. Superimposition of two-dimensional ^{1}H, ^{15}N HSQC spectra of ^{15}N-tau (in red) with ^{15}N-tau mixed with non-labelled VHH F8-$2_{S54L\ T128A}$ (overlaid in blue). **b.** Spectra enlargements show broadened resonances corresponding to residues implicated in the interaction

c. Normalized intensities I/I0 of corresponding resonances in the two-dimensional spectra of tau with equimolar quantity of VHH F8-$2_{S54L\ T128A}$ (I) or free in solution (I0) for residues along the tau sequence. Overlapping resonances are not considered (x-axis is not scaled).

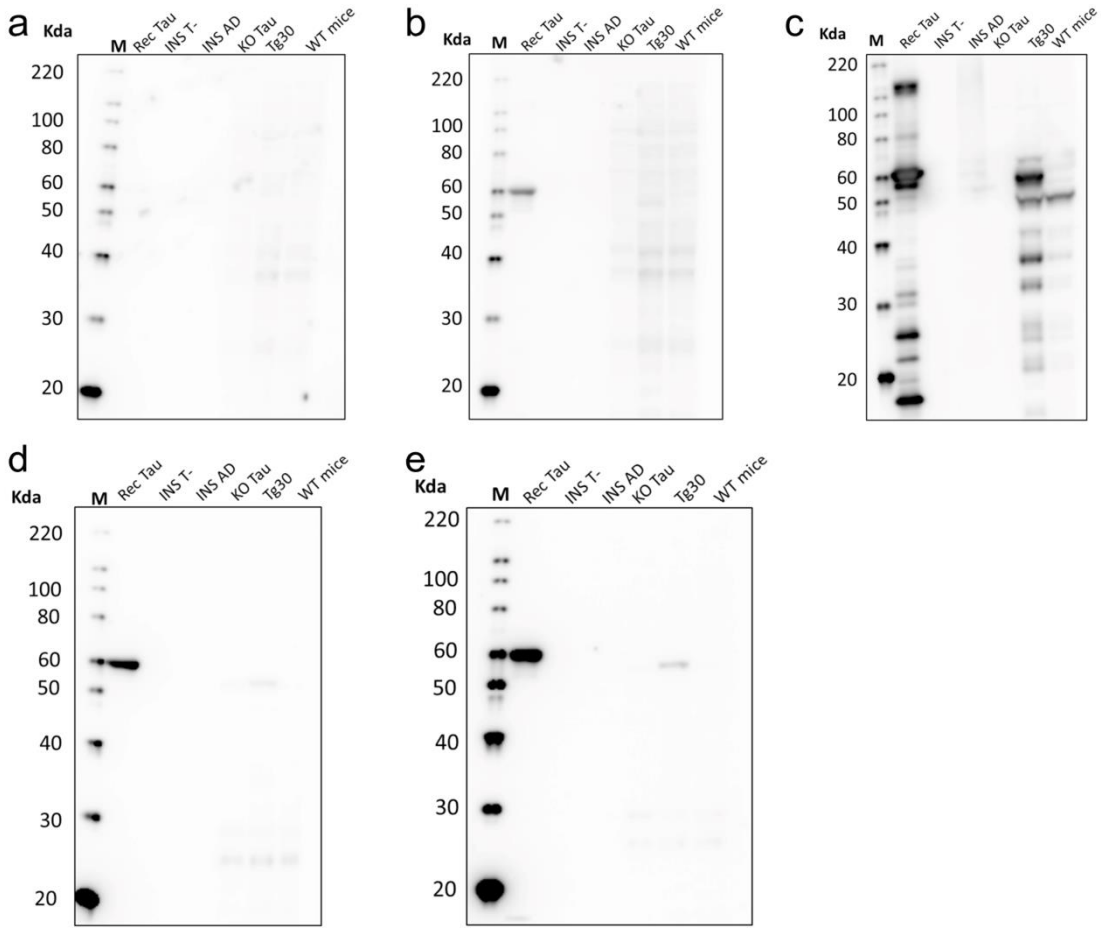


Fig. S10 :Full blots corresponding to the details of the immunodetection analysis shown in **Fig. 7.**
Loaded samples correspond to recombinant 2N4R tau (Rec Tau), sarkosyl insoluble fraction from a human control brain (INS T-), sarkosyl insoluble fraction from an AD brain patient (INS AD), brain lysate from transgenic KO-tau mouse model (KO Tau), from transgenic ThyTau30 mouse model (Tg30) and wild-type mice (WT mice).
a. anti-VHH antibody labeling only (secondary antibody control), **b.** VHH F8-2_{R111C} labeling, **c.** anti-tau Cter (positive control). For RecTau and Tg30 samples, the bands observed at lower molecular weights compare to the 60kDa tau2N4R most probably correspond to binding of the antibody to tau fragments (except for the band corresponding to wild type mouse tau in the Tg30 and WT mouse samples). For RecTau, the bands observed at higher molecular weight compare to the 60kDa tau2N4R is most probably due to tau multimers recognition, **d.** minibody F8-2_{R111C} labeling and **e.** minibody F8-2_{S54L} labeling .

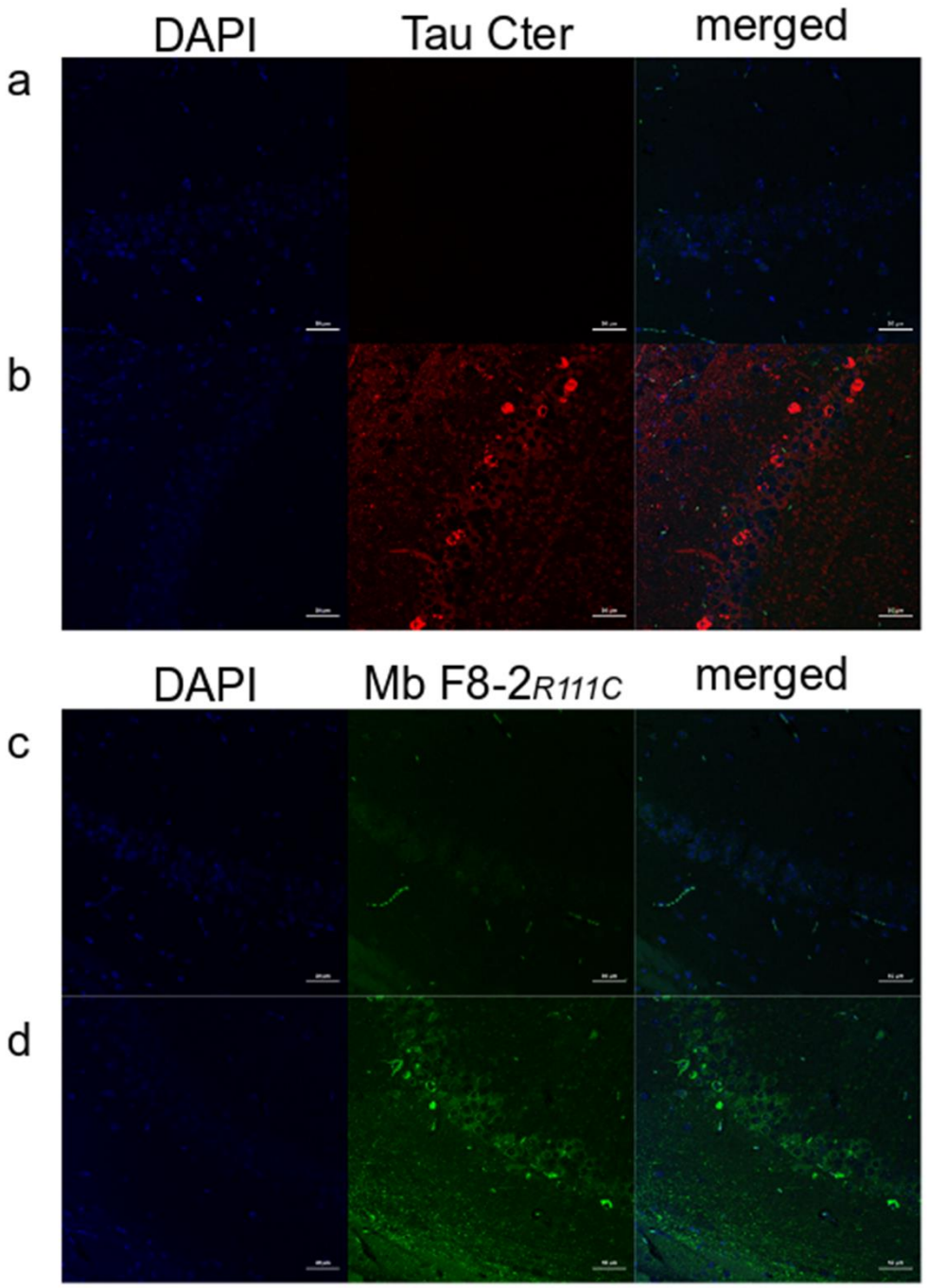


Fig.S11 :
Immunofluorescence labeling of tau in the CA1 layer of hippocampus from **a.** transgenic KO-Tau and **b**. THY-Tau30 mice revealed by an anti-tau Cter.

Immunofluorescence labeling of tau in the CA1 layer of hippocampus from **c.** transgenic KO-Tau and **d.** THY-Tau30 mice revealed by minibody F8-2_{R111C}. The labellng is conserved compared to Fig. 7, showing that there was no interference between antibodies when they are simultaneously used for detection.

oli6690 CAGGGCAATAAAGTCGAACT, Oli6972 GACCTACAGGAAAGAGTTACTC,

oligo 6972 GACCTACAGGAAAGAGTTACTC

oli10829
CTATTCGATGATGAAGATACCCCACCAAACCCAAAAAAAAGAGATCCTAGAACTAGACACTCTTTCCCT
ACACGACGCTCTTCC,

oli10830
CCGGGCCTCTAGACACTAGCTACTCGAGGGGCCCCAGTGGCCCTATCTATGCGGCCGCTCAGACTGG
AGTTCAGACGTGTGCTC

SI12: oligonucleotide sequences (5’ to 3’ orientation) used for PCR amplification of tau cDNA

oli3390
5pTCTGCACAATATTTCAAGCTATACCAAGCATACAATCAACTCCAAGCTAGAACCATGGCGGAAGTGCAG
CTGCAGGCTC

oli3880
3pTCTTCTTTTTTGGAGGCTCGGGAATTAATTCCGCTTTATCCATCTTTGCGGCGGCCGCGCTACTCAC
AGTTACCTG

SI13: oligonucleotide sequences used for PCR amplification of VHH F8-2